PHYSICAL REVIEW D **96,** 096014 (2017)

Edge states and thermodynamics of rotating relativistic fermions under magnetic field

M. N. Chernodub[1,2] and Shinya Gongyo[3]

[1]*Laboratoire de Mathématiques et Physique Théorique UMR 7350, Université de Tours, Tours 37200 France*

[2]*Laboratory of Physics of Living Matter, Far Eastern Federal University, Sukhanova 8, Vladivostok, 690950, Russia*

[3]*Theoretical Research Division, Nishina Center, RIKEN, Wako, Saitama 351-0198, Japan*

(Received 29 June 2017; published 17 November 2017)

We discuss free Dirac fermions rotating uniformly inside a cylindrical cavity in the presence of background magnetic field parallel to the cylinder axis. We show that, in addition to the known bulk states, the system contains massive edge states with the masses inversely proportional to the radius of the cylinder. The edge states appear at quantized threshold values of the fermion mass, which depend on the details of (chiral) MIT boundary conditions imposed at the surface of the cylinder. In the limit of infinite fermion mass, the masses of the edge states remain finite but, generally, nonzero as contrasted to the masses of the bulk states which become infinitely large. The presence of magnetic field affects the spectrum of both bulk and edge modes, and the masses of the edge states may vanish at certain quantized values of magnetic field. The moment of inertia of Dirac fermions is nonmonotonically increasing, oscillating function of magnetic field. The oscillations are well pronounced in a low-temperature domain and disappear at high temperatures. We also show that the edge modes alone do not support the anomalous transport phenomena such as chiral magnetic and chiral vortical effects.

DOI: 10.1103/PhysRevD.96.096014

I. INTRODUCTION

Rotating systems of relativistic fermions appear in various physical settings characterized by different energy scales. The examples include the interior of rapidly spinning neutron stars [1], quark-gluon plasma in noncentral heavy-ion collisions [2], and anomalous-vortical chiral transport phenomena [3] applied both to neutrino fluxes in rotating astrophysical environments [4,5] and to semimetal materials in solid-state applications [6].

Rotation changes the spectrum of free fermions [7–11] and, consequently, affects the mass gap generation in interacting fermionic systems. For example, the critical temperature of chiral symmetry restoration T_c is a diminishing function of the rotational angular frequency Ω [12–16]. The rotational effects have been studied under the simplifying assumption that the rotation is globally uniform so that the angular velocity does not depend on the distance to the rotational axis. A uniformly rotating relativistic system should be bounded in the transverse directions with respect to the axis of rotation in order to comply with the causality principle. The latter requires that the velocity of particles should not exceed the speed of light to avoid pathological effects [9,17]. The presence of the boundary implies a dependence of the chiral restoration temperature $T_c = T_c(\Omega)$ on geometrical features, in particular, on the type of the boundary condition [18]. The uniform rotation in magnetic field background but in an unrestricted transverse geometry has been studied in Ref. [13].

In this paper, we generalize the results of Refs. [10,18] in threefold way. First, we show that, in addition to the bulk modes, the spectrum of free massive Dirac fermions contains the edge states localized at the boundary of the cylinder. Second, we discuss the spectrum of both bulk and edge modes in the presence of external magnetic field. Finally, we illustrate the importance of the edge modes for thermodynamics of free Dirac fermions and for its rotational properties such as the moment of inertia which exhibits curious oscillating behavior as a function of magnetic field.

Notice that possible effects of the edge states have not been accounted for in existing studies of the phase structure of the interacting rotating fermions [13–16,18]. In Refs. [13,14], rotational properties were investigated in the transversally unrestricted geometry which questions the consistency with the requirement of relativistic causality under uniform rotation and, simultaneously, does not allow for the presence of the edge states. The existence of the edge states, found in the present paper, definitely calls for a reestimation of the phase diagram of interacting fermions under uniform rotation.

We would like to mention that in solid-state terms the system of Dirac fermions considered in this article corresponds to a nontopological insulator as it is characterized by the presence of gapped bulk modes and the absence of symmetry-protected boundary (edge) states with zero mass. The edge states are generally massive, and their mass is proportional to the mean curvature of the cylinder

surface. Notice that the Dirac equation alone is not enough to describe topological insulators [19], where the presence of zero-mass edge states is guaranteed by topological reasons of underlying lattice Hamiltonians [20].

The structure of this paper is as follows. In Sec. II, we review, following Ref. [10], known bulk solutions for the Dirac fermions in the cylinder with the MIT boundary conditions in the absence of magnetic field. We also discuss particularities of the spectrum for the chiral boundary conditions [18]. In the same section, we find the edge states of the system and describe their properties. In Sec. III, we discuss properties of bulk and edge solutions in the magnetic field background. Section IV is devoted to studies of rotational properties of the system in the limit of (negative) infinite fermion mass. In this limit, the thermodynamics of the system is given by the edge states only, allowing us to highlight their importance. We also demonstrate explicitly that the edge modes cannot lead to anomalous transport phenomena such as chiral magnetic and chiral vortical effects. The last section is devoted to conclusions.

II. BULK AND EDGE SOLUTIONS IN THE ABSENCE OF MAGNETIC FIELD

In this section, we discuss solutions of massive rigidly rotating Dirac fermions confined in a cylindrical geometry in the absence of magnetic field. We start from the known bulk states that were already described in Ref. [10] (see also Ref. [15]), and then we demonstrate that the system contains also certain new (edge) states which possess rather peculiar properties.

A. Dirac equation in the cylinder

We consider a system of free fermions which is rigidly rotating with the angular frequency Ω about the axis of the infinitely long cylinder of the radius R.

Given the geometry of the system, it is convenient to work in the cylindrical coordinates, $x \equiv (t, x, y, z) = (t, \rho\cos\varphi, \rho\sin\varphi, z)$. There are two natural reference frames in this problem: the inertial laboratory frame and noninertial corotating frame. The former one corresponds to a rest frame, while the latter one is rigidly fixed with the rotating system. The coordinates t, ρ, and z in the corotating reference frame coincide with the corresponding coordinates of the laboratory frame: $t = t_{\rm lab}$, $\rho = \rho_{\rm lab}$, and $z = z_{\rm lab}$. The angular variables in these frames are related as

$$\varphi = [\varphi_{\rm lab} - \Omega t]_{2\pi}, \tag{1}$$

where $[\ldots]_{2\pi}$ means "modulo 2π." The simple relation between angular variables (1) leads, nevertheless, to a quite nontrivial metric in the corotating frame,

$$g_{\mu\nu} = \begin{pmatrix} 1-(x^2+y^2)\Omega^2 & y\Omega & -x\Omega & 0 \\ y\Omega & -1 & 0 & 0 \\ -x\Omega & 0 & -1 & 0 \\ 0 & 0 & 0 & -1 \end{pmatrix}, \tag{2}$$

which corresponds to the line element

$$\begin{aligned} ds^2 &= g_{\mu\nu}dx^\mu dx^\nu = \eta_{\hat\mu\hat\nu}dx^{\hat\mu}dx^{\hat\nu} \\ &= (1-\rho^2\Omega^2)dt^2 - 2\rho^2\Omega dt d\varphi - d\rho^2 - \rho^2 d\varphi^2 - dz^2, \end{aligned} \tag{3}$$

where $\eta_{\hat\mu\hat\nu} = \mathrm{diag}(1,-1,-1,-1)$ is the flat metric. Here, we adopt the convention that $\hat\imath, \hat\jmath \ldots = \hat t, \hat x, \hat y, \hat z$ and $\mu, \nu \ldots = t,\ x,\ y,\ z$ refer to the local coordinates in the laboratory frame and the corotating frame, respectively. We use the units in which the speed of light and the reduced Planck constant are equal to unity, $c = \hbar = 1$.

The spectrum of the fermions is described by the eigenfunctions of the free Dirac equation in the corotating reference frame [10],

$$[i\gamma^\mu(\partial_\mu + \Gamma_\mu) - M]\psi = 0, \tag{4}$$

where the Dirac matrices in the curved corotating spacetime $\gamma^\mu(x) = e^\mu_{\hat\imath}(x)\gamma^{\hat\imath}$ are connected to the matrices in the laboratory frame $\gamma^{\hat\imath}$ via the vierbein $e^\mu_{\hat\imath}$. The vierbein is a "square root" of the metric $\eta_{\hat\imath\hat\jmath} = g_{\mu\nu}e^\mu_{\hat\imath}e^\nu_{\hat\jmath}$. In the case of the metric (2), the vierbein may be chosen in the form

$$e^t_{\hat t} = e^x_{\hat x} = e^y_{\hat y} = e^y_{\hat y} = 1, \quad e^x_{\hat t} = y\Omega, \quad e^y_{\hat t} = -x\Omega, \tag{5}$$

with all other components of $\eta_{\hat\imath\hat\jmath}$ being zero.

In Eq. (4), the spin connection Γ^μ in the metric (2) has only one nonzero component,

$$\Gamma_t = -\frac{i}{2}\Omega\sigma^{\hat x\hat y}, \tag{6}$$

where

$$\sigma^{\hat x\hat y} \equiv \Sigma_z = \begin{pmatrix} \sigma^3 & 0 \\ 0 & \sigma^3 \end{pmatrix} \tag{7}$$

in the Dirac representation of the gamma matrices:

$$\gamma^{\hat t} = \begin{pmatrix} \mathbb{1} & 0 \\ 0 & -\mathbb{1} \end{pmatrix}, \quad \gamma^{\hat\imath} = \begin{pmatrix} 0 & \sigma_i \\ -\sigma_i & 0 \end{pmatrix}, \quad \gamma^5 = \begin{pmatrix} 0 & \mathbb{1} \\ \mathbb{1} & 0 \end{pmatrix}. \tag{8}$$

Equation (4) is supplemented with the MIT boundary condition at the boundary of the cylinder,

$$i\gamma^\mu n_\mu(\varphi)\psi(t,z,R,\varphi) = \psi(t,z,R,\varphi), \tag{9}$$

where the spatial vector $n_\mu(\varphi) = (0, \cos\varphi, \sin\varphi, 0)$ is normal to the cylinder surface. This condition "confines" the fermions inside the cavity by enforcing the normal component $j_{\boldsymbol{n}} \equiv -j^\mu n_\mu$ of the fermionic current $j^\mu = \bar\psi\gamma^\mu\psi$ to vanish at the surface of the cylinder $j_{\boldsymbol{n}}(\rho = R) = 0$. Furthermore, the condition (9) implies that the chiral condensate, $\bar\psi\psi$, and the axial current along the z direction, j^5_z, vanish at the surface of the cylinder:

$$\bar\psi\psi|_{\rho=R} = 0, \qquad j^5_z(\rho = R) \equiv \bar\psi\gamma^5\gamma^{\hat z}\psi|_{\rho=R} = 0. \quad (10)$$

B. Bulk states

A general solution of the Dirac Eq. (4) in the (co)rotating reference frame (1) has the form (according to Ref. [10])

$$U^\lambda_j = \frac{1}{2\pi} e^{-i\tilde E t + ikz} u^\lambda_j(\rho, \varphi), \quad (11)$$

where u^λ_j is an eigenspinor characterized by the eigenstate helicity $\lambda = \pm 1/2$, the z component of momentum $k \equiv k_z \in \mathbb{R}$, the projection of the quantized angular momentum $m \equiv m_z \in \mathbb{Z}$ onto the z axis, and the radial quantum number $l = 1, 2, \ldots$, which describes the behavior of the solution in terms of the radial ρ coordinate. The helicity λ of the state is the eigenvalue of the helicity operator $\hat W = \hat P \cdot \hat{\boldsymbol{J}}/p$,

$$\hat W U^\lambda_{Ekm} = \lambda U^\lambda_{Ekm}, \quad (12)$$

where $\hat P = -i\boldsymbol{\partial}$ is the momentum operator and $\hat J$ is the angular momentum operator. In the absence of magnetic field, the helicity operator $\hat W$ has the simple form

$$\hat W = \begin{pmatrix} \hat h & 0 \\ 0 & \hat h \end{pmatrix}, \qquad \hat h = \frac{\boldsymbol{\sigma}\cdot\hat{\boldsymbol{P}}}{2p}, \quad (13)$$

where $p \equiv \sqrt{E^2 - M^2} > 0$ is the magnitude of the spatial momentum defined as follows:

$$\hat{\boldsymbol{P}}^2 U^\lambda_j = p_j^2 U^\lambda_j. \quad (14)$$

Here, the notation

$$j = (k, m, l), \quad (15)$$

is used to denote a set of quantum numbers [10].

The energy in the corotating frame $\tilde E_j$ is related to the energy E_j in the laboratory frame as

$$\tilde E_j = E_j - \Omega\left(m + \frac{1}{2}\right) \equiv E_j - \Omega\mu_m, \quad (16)$$

where μ_m can be identified with the quantized value of the z component of the total angular momentum

$$\hat J_z\psi = \mu_m\psi, \qquad \mu_m = m + \frac{1}{2}, \quad (17)$$

which comprises the orbital and spin parts,

$$\hat J_z = -i\partial_\varphi + \frac{1}{2}\Sigma_z, \quad (18)$$

where the matrix Σ_z is given in Eq. (7).

The solutions of the Dirac equation which satisfy the MIT boundary conditions (9) are linear combinations of positive and negative helicity spinors,

$$U^{\rm MIT}_j = \mathcal{C}^{\rm MIT}_j[\mathsf{b}U^+_j + U^-_j], \quad (19)$$

where the 4-spinors with a definite helicity λ,

$$u^\lambda_j(\rho, \varphi) = \frac{1}{\sqrt{2}}\begin{pmatrix} \mathsf{E}_+\phi^\lambda_j \\ \frac{2\lambda E_j}{|E_j|}\mathsf{E}_-\phi^\lambda_j \end{pmatrix}, \quad (20)$$

are expressed with the 2-spinors

$$\phi^\lambda_j(\rho, \varphi) = \frac{1}{\sqrt{2}}\begin{pmatrix} \mathsf{p}_\lambda e^{im\varphi} J_m(q\rho/R) \\ 2i\lambda\mathsf{p}_{-\lambda} e^{i(m+1)\varphi} J_{m+1}(q\rho/R) \end{pmatrix}, \quad (21)$$

which are eigenspinors of the two-component helicity operator $\hat h$ (13),

$$\begin{pmatrix} k_j & \hat P_- \\ \hat P_+ & -k_j \end{pmatrix}\frac{\phi_j(\rho, \phi)}{2p_j} = \lambda_j\phi_j(\rho, \phi), \quad (22)$$

with $\hat P_\pm = \hat P_x \pm i\hat P_y = -ie^{\pm i\varphi}(\partial_\rho \pm i\rho^{-1}\partial_\varphi)$.

In the eigenfunctions (19), the degree of mixing between positive and negative helicity states is determined by the parameter

$$\mathsf{b} = \frac{\mathsf{E}_+\mathsf{p}_+ + \mathsf{E}_-\mathsf{p}_-\mathsf{j}_{ml}\,\mathrm{sign}(E_j)}{\mathsf{E}_+\mathsf{p}_- + \mathsf{E}_-\mathsf{p}_+\mathsf{j}_{ml}\,\mathrm{sign}(E_j)}, \quad (23)$$

where

$$\mathsf{p}_\pm \equiv \mathsf{p}_{\pm 1/2} = \sqrt{1 \pm \frac{k}{p_j}},$$
$$\mathsf{E}_\pm \equiv \mathsf{E}_{\pm 1/2} = \sqrt{1 \pm \frac{M}{E_j}} \quad (24)$$

are, respectively, the momentum- and energy-related quantities which depend explicitly on the helicity of the eigenmodes and

$$p_j = \sqrt{k^2 + \frac{q^2_{ml}}{R^2}} \quad (25)$$

is (the modulus of) the effective momentum which incorporates the longitudinal continuous momentum k and the transverse (radial) discrete momentum number $q \equiv q_{ml}$. We also use the notation [10]

$$\mathrm{j}_{ml} = \frac{J_m(q_{ml})}{J_{m+1}(q_{ml})}, \tag{26}$$

where $J_m(x)$ is the Bessel function.

The dimensionless real-valued and positive quantity q_{ml} is the lth real-valued positive root $(l = 1, 2, \ldots)$ of the following equation [10]:

$$J_m^2(q) + \frac{2MR}{q} J_m(q) J_{m+1}(q) - J_{m+1}^2(q) = 0. \tag{27}$$

The normalization coefficient

$$\mathcal{C}_j^{\mathrm{MIT}} = \frac{1}{R|J_{m+1}(q_{m,l}R)|} \cdot \sqrt{\frac{\mathsf{p}_-^2 + \mathsf{p}_+^2 \mathrm{j}_{ml}^2}{(\mathrm{j}_{ml}^2+1)(\mathrm{j}_{ml}^2 - (2m+1)\frac{\mathrm{j}_{ml}}{q_{m,l}R} + 1) - (\mathrm{j}_{ml}^2 - 1)\frac{\mathrm{j}_{ml}}{q_{m,l}R}}} \tag{28}$$

ensures that these modes are orthonormalized,

$$\langle U_j^{\mathrm{MIT}}, U_{j'}^{\mathrm{MIT}} \rangle = \delta(k-k')\delta_{m,m'}\delta_{l,l'}\theta(E_j E_{j'}), \tag{29}$$

with respect to the inner Dirac product:

$$\langle \psi, \chi \rangle = \int_{-\infty}^{+\infty} dz \int_0^{2\pi} d\varphi \int_0^R d\rho \rho \psi^\dagger(x)\chi(x). \tag{30}$$

The energies of the eigenmodes in the laboratory frame are

$$E_j \equiv E_{ml}(k, M) = \pm\sqrt{k^2 + M^2 + \frac{q_{ml}^2}{R^2}}, \tag{31}$$

where the plus (minus) sign corresponds to the particle (antiparticle) modes.

The density $\bar{\psi}\gamma^0\psi \equiv \psi^\dagger\psi$ of the wave functions (20) is not localized at the boundary of the cylinder, and therefore we refer to these solutions as the "bulk eigenmodes." They should be discriminated from the "edge" solutions (to be discussed below) for which the density is concentrated at the boundary of the cylinder. From Eq. (31), we conclude that the masses of the bulk states M^{bulk} defined as

$$M_{ml}^{\mathrm{bulk}} = \sqrt{M^2 + \frac{q_{ml}^2}{R^2}} \tag{32}$$

are higher than or equal to the mass of the fermion M.

The reflection $m \to -1-m$, corresponding to the sign flips of the total angular momentum (17) $\mu_m \to -\mu_m$, leaves the q_{ml} solutions unchanged,

$$q_{ml} \to q_{-1-m,l} \equiv q_{ml}. \tag{33}$$

This property implies that the mass spectrum (32) and, consequently, the energy spectrum of the bulk modes are invariant under the flips $\mu_m \to -\mu_m$.

A couple of real-valued solutions q_{ml} of Eq. (27) are shown in Fig. 1(a) as a function of the fermion mass M. As the mass M decreases, the lowest $(l = 1)$ real-valued modes $q_{ml} \geq 0$ touch the $q = 0$ axis and disappear one by one at the critical values of the (negative) fermion mass:

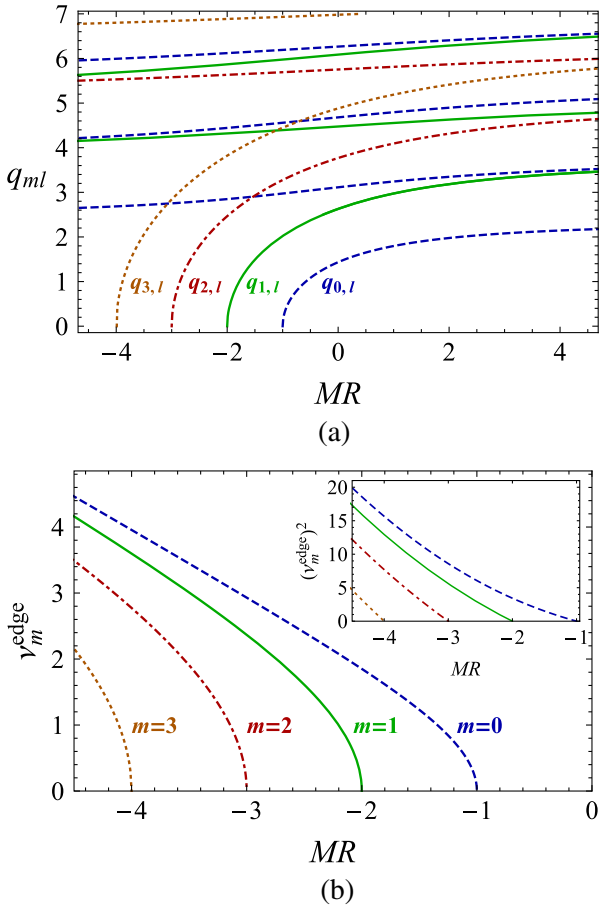

FIG. 1. (a) Solutions of the eigenvalue Eq. (27) as the function of the fermion mass M: (a) the real-valued solutions $q \geq 0$ corresponding to the bulk modes (from Ref. [15]) and (b) the purely imaginary solutions $q^{\mathrm{edge}} = i\nu^{\mathrm{edge}}$ with $\nu \geq 0$ corresponding to the edge modes. The inset shows $(\nu^{\mathrm{edge}})^2$ vs M.

$$M_c^{(m)} = -\frac{1}{R}\left(|\mu_m| + \frac{1}{2}\right) \equiv \begin{cases} -\frac{1+m}{R}, & m \geq 0, \\ \frac{m}{R}, & m < 0. \end{cases} \quad (34)$$

As the values $q_{m,1}$ and $q_{-1-m,1}$ coincide with each other due to the reflection invariance (33), the real-valued q will disappear in pairs at the critical mass points (34). Contrary to the ground state with $l = 1$, the excited $l \geq 1$ bulk states do not disappear from the spectrum.

Finally, we would like to stress that the values of the critical mass (34) depend on the type of the boundary condition at the boundary of the cylinder. For example, if we flip the sign of the vector n_μ in the MIT boundary condition (9), then the mass critical values (34) would also change the sign, $M_c^{(m)}(-n_\mu) = -M_c^{(m)}(n_\mu)$, so that the disappearance of the ground-state ($l = 1$) modes would then happen at the positive fermion masses, $M_c^{(m)} > 0$. With the more general chiral boundary conditions parametrized by the chiral angle Θ [21],

$$[i\gamma^\mu n_\mu(\varphi) - e^{-i\Theta\gamma^5}]\psi(t, z, \rho, \varphi)|_{\rho=R} = 0, \quad (35)$$

the critical masses becomes as follows [18]:

$$M_c^{(m)}(\Theta) = \frac{M_c^{(m)}(0)}{\cos\Theta} \equiv \begin{cases} -\frac{1+m}{\cos\Theta}\frac{1}{R}, & m \geq 0, \\ \frac{m}{\cos\Theta}\frac{1}{R}, & m < 0. \end{cases} \quad (36)$$

In particular, at the specific values of the chiral angle $\Theta = \pm\pi/2$, the ground-state levels never disappear.

C. Edge states

Besides the bulk eigenfunctions with real-valued solution $q = q_{ml}$, the system contains also quite peculiar eigenstates, which are localized at the boundary of the cylinder. These are the edge states which correspond to purely imaginary solutions of Eq. (27),

$$q_m^{\text{edge}} = i\nu_m^{\text{edge}}, \quad (37)$$

with a real $\nu_m^{\text{edge}} \geq 0$.[1]

Using the relation $J_m(ix) = i^m I_m(x)$, we get from Eq. (27) the equation which determines ν,

$$I_m^2(\nu) + \frac{2MR}{\nu} I_m(\nu) I_{m+1}(\nu) + I_{m+1}^2(\nu) = 0, \quad (38)$$

where $I_m(x)$ is the modified Bessel function.

In Fig. 1(b), we show the solutions of Eq. (38) as the function of the fermion mass M. First of all, we notice that there is only one edge eigenmode for each value of the orbital momentum m. Moreover, the edge modes ν_m^{edge} appear at the critical mass points (34) where the lowest bulk modes $q_{m,1}$ disappear (as the fermion mass M diminishes). Therefore, we conclude that at the critical mass points (34) the lowest bulk modes (34) are transformed into the edge modes and vise versa.

Despite that the edge states appear at negative values of the fermion mass M, these solutions represent physical modes which contribute to the equation of state and other thermodynamic properties of the system (certain examples will be considered in Sec. IV below). One can show, for instance, that the negative critical values (34) flip their signs $M_c^{(m)} \to -M_c^{(m)}$ if the spatial vector $\boldsymbol{n}$ in the MIT boundary condition (9) is flipped from the outward direction to the inward direction, $\boldsymbol{n} \to -\boldsymbol{n}$. Both original and flipped MIT boundary conditions have apparently the same physical sense, as they confine fermions inside the cylinder. The MIT boundary condition with flipped vector $\boldsymbol{n}$ corresponds to the "chiral boundary condition" considered for the case of the cylinder in Ref. [10]:

$$[i\gamma^\mu n_\mu(\varphi) + 1]\psi(t, z, \rho, \varphi)|_{\rho=R} = 0. \quad (39)$$

The sign flip of the fermion mass is related to the chiral transformation

$$\psi \to e^{-i\theta\gamma_5}\psi, \qquad \bar{\psi} \to \bar{\psi}e^{-i\theta\gamma_5} \quad (40)$$

of the Dirac spinors. This transformation leads to the modification of the mass term

$$M \to e^{-i\theta\gamma_5} M e^{-i\theta\gamma_5} \quad (41)$$

of the Dirac Eq. (4). The choice $\theta = \pi/2$ changes the sign of the fermion mass, $M \to -M$, while not affecting the sign of energy of the eigenmode (42). In an infinite volume, the positive and flipped negative fermionic masses correspond to the same *positive-energy* particle state related by the discrete ($\theta = \pi/2$) chiral transformation (40). In a cylindric cavity, the MIT boundary condition (9) breaks down the chiral symmetry (40) explicitly, thus leading to the asymmetry of the fermionic spectrum with respect to the flip of the fermion mass. In other words, the would-be inequivalence of features of fermions with positive and negative masses is caused by the MIT boundary condition which breaks explicitly the chiral flip symmetry $M \to -M$.

The energy E_j of the edge states in the laboratory frame is

$$E_j^{\text{edge}} = \pm\sqrt{p_j^2 + M^2} \equiv \pm\sqrt{k^2 + (M_m^{\text{edge}})^2}, \quad (42)$$

where

$$p_j = \sqrt{k^2 - \frac{\nu_m^2}{R^2}} \quad (43)$$

[1] As in the case of the bulk modes, the solutions ν_m^{edge} and $-\nu_m^{\text{edge}}$ correspond to the same eigenmode.

is an analog of momenta. The plus (minus) sign in Eq. (42) corresponds to the particle (antiparticle) modes similarly to the bulk modes (31).

Equation (42) implies that, contrary to the masses of the bulk states (32), the masses of the edge states are smaller than or equal to the mass of the fermion M:

$$M_m^{\rm edge} = \sqrt{M^2 - \frac{\nu_m^2}{R^2}}. \tag{44}$$

Notice that, due to the inequality $|\nu_m| < MR$, the masses (44) of the edge states and their energies $E^{\rm edge}$ always remain real numbers, while the effective momentum p may take become purely imaginary for longitudinal momenta $|k| < \nu_m/R$. In other words, for the edge modes, $\nu_m^2 > 0$, $k^2 > 0$, and $E_j^2 > 0$, while p_j^2 may take both positive and negative values. The negative values of the effective momentum squared p_j^2 are not consistent with the real-valued spectrum of the helicity operator (13) due to the anti-Hermiticity of this operator. Nevertheless, as we will see shortly, we may apply to the edge modes all the steps of the derivation of Sec. II B following Ref. [10]. The presence of the edge modes is largely related to the helicity-broken boundary conditions at the edge of the cylinder. Namely, the MIT boundary conditions (9) couple the modes with different helicity λ, Eq. (19), so that the general eigenmode solution (19) mixes both $\lambda = \pm$ helicities. As a consequence, the edge eigenmodes do not possess a definite helicity at all.

In the rotating frame, the energy of the edge mode follows from Eq. (16),

$$\tilde{E}_j^{\rm edge} = E_j^{\rm edge} - \Omega\mu_m, \tag{45}$$

where $E_j^{\rm edge}$ is the energy of the edge modes in the laboratory frame (42).

In Fig. 2, we show the mass spectrum both for the bulk modes (32) and for the edge modes (44). This figure clearly demonstrates that the ground state $l = 1$ becomes the edge mode as the critical point (34) is passed for each fixed m.

Similarly to the bulk modes (33), a reflection in the sign of the total angular momentum (17), $\mu_m \to -\mu_m$, leaves the ν_{ml} eigenvalues unchanged,

$$q_{ml} \to q_{-1-m,l} \equiv q_{ml}. \tag{46}$$

Therefore, the energy spectrum of the edge modes is symmetric with respect to the flips $\mu_m \to -\mu_m$. Both bulk and edge modes are degenerate in the absence of external magnetic field.

The 2-spinors of the edge eigenmode with definite helicity λ are given the spinor

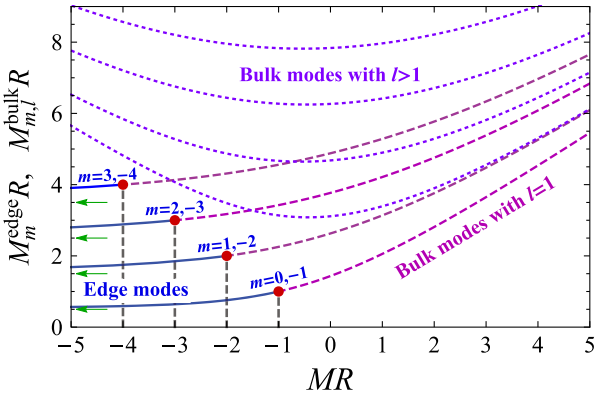

FIG. 2. The masses (44) of the edge states (the solid blue lines) and the masses (32) of the lowest ($l = 1$) bulk states (the dashed magenta lines) as the function of the fermion mass M in the absence of magnetic field, $B = 0$. Four lowest states are shown. The critical points (34) are marked by the red dots (and the thin gray lines). The asymptotic masses of the edge states (76) in the limit $M \to -\infty$ are shown by the green arrows. Four lowest $l > 1$ bulk states are shown by the dotted lines.

$$\phi_\lambda = C_\phi^j \check{\phi}_\lambda, \qquad \check{\phi}_\lambda = \begin{pmatrix} (k + 2p_j\lambda) e^{im\varphi} I_m(\nu_m \frac{\rho}{R}) \\ -i\frac{\nu_m}{R} e^{i(m+1)\varphi} I_{m+1}(\nu_m \frac{\rho}{R}) \end{pmatrix}, \tag{47}$$

where C_ϕ^j is a normalization constant and we implied that the check mark over a spinor means that this spinor is not normalized.

To prove that the spinor (47) is the eigenmode of the helicity operator (22), we used the useful relations

$$\hat{P}_+ \left[e^{im\varphi} I_m\left(\nu_m \frac{\rho}{R}\right)\right] = \frac{\nu_m}{iR} e^{i(m+1)\varphi} I_{m+1}\left(\nu_m \frac{\rho}{R}\right), \tag{48}$$

$$\hat{P}_- \left[e^{i(m+1)\varphi} I_{m+1}\left(\nu_m \frac{\rho}{R}\right)\right] = \frac{\nu_m}{iR} e^{im\varphi} I_m\left(\nu_m \frac{\rho}{R}\right) \tag{49}$$

for the operators

$$\hat{P}_\pm = -ie^{\pm i\varphi}(\partial_\rho \pm i\rho^{-1}\partial_\varphi). \tag{50}$$

The 2-spinors for the bulk modes (21) were normalized using the condition [10],

$$\sum_{m\in Z} \phi_{Ekm}^{\lambda,\dagger} \phi_{Ekm}^{\lambda} = 1, \tag{51}$$

which utilized the convenient summation property of the Bessel functions:

$$\sum_{m\in\mathbb{Z}} J_m^2(x) = 1. \tag{52}$$

The edge states (47) depend on modified, rather than usual, Bessel functions that possess a different summation rule:

$$\sum_{m\in\mathbb{Z}}(-1)^m I_m^2(x)=1. \tag{53}$$

This equations suggests that the edge eigenmodes (47) should be normalized according to another normalization relation,

$$\sum_{m\in Z}(-1)^m \phi^{\mathrm{edge},\dagger}_{Ekm}\phi^{\mathrm{edge}}_{Ekm}=1, \tag{54}$$

which has a less clear physical sense. Nevertheless, for the sake of completeness, we give the value of the prefactor C^j_ϕ corresponding to the normalization (54):

$$\begin{aligned} C^j_\phi &= \frac{1}{\sqrt{2}}\frac{1}{\sqrt{k^2+2\lambda k\mathrm{Re}p_j+\mathrm{Im}^2 p_j}} \\ &= \frac{1}{\sqrt{2}}\cdot\begin{cases}(k^2+2\lambda k p_j)^{-1/2}, & p_j^2>0,\\ R/\nu_m, & p_j^2<0.\end{cases}\end{aligned} \tag{55}$$

In the corotating reference frame, the Dirac equation, if expressed via the corotating coordinates, has the same form as the standard Dirac equation in the laboratory frame in the absence of rotation. Using the explicit representation of the γ matrices (8), the Dirac Eq. (4) in the corotating frame can be rewritten as

$$(i\partial\!\!\!/ - M)U^{\mathrm{edge}}_{j,\lambda}\equiv\begin{pmatrix}E^{\mathrm{edge}}_j - M & -2p_j\hat{h}\\ 2p_j\hat{h} & -(E^{\mathrm{edge}}_j+M)\end{pmatrix}U^{\mathrm{edge}}_{j,\lambda}=0$$

or

$$\begin{pmatrix}E^{\mathrm{edge}}_j - M & -2p_j\lambda\\ 2p_j\lambda & -(E^{\mathrm{edge}}_j+M)\end{pmatrix}\Psi^{\mathrm{edge}}_{j,\lambda}=0, \tag{56}$$

where we set

$$\begin{aligned} U^{\mathrm{edge}}_{j,\lambda} &= \frac{1}{2\pi}e^{-i\tilde{E}^{\mathrm{edge}}_j t+ikz}\Psi^{\mathrm{edge}}_{j,\lambda},\\ \Psi^{\mathrm{edge}}_{j,\lambda} &= \begin{pmatrix}C^{\lambda,\mathrm{up}}_j\check{\phi}^\lambda_j\\ C^{\lambda,\mathrm{down}}_j\check{\phi}^\lambda_j\end{pmatrix}\end{aligned} \tag{57}$$

and then used the fact that the 2-spinors $\check{\phi}^\lambda_j$, Eq. (47), are the eigenfunctions of the helicity operator $\hat{h}$, Eq. (13).

The self-consistency of the Dirac equation for the edge modes (56) gives us the expression for their energy (42) and fixes the coefficients $C^{\lambda,\mathrm{up}}_j$ and $C^{\lambda,\mathrm{down}}_j$ in Eq. (57) up to the overall normalization factor (set to unity in this expression):

$$\check{\Psi}^{\mathrm{edge}}_{j,\lambda}=\begin{pmatrix}(E^{\mathrm{edge}}_j+M)\check{\phi}^\lambda_j\\ 2\lambda p_j\check{\phi}^\lambda_j\end{pmatrix}. \tag{58}$$

Denoting $\Psi^{\mathrm{edge}}_j=(\Psi^j_\uparrow,\Psi^j_\downarrow)^T$, the MIT boundary conditions (9) may be explicitly written as

$$(i\not{n}-1)\Psi^{\mathrm{edge}}_j=-\begin{pmatrix}\mathbb{1} & i\sigma^\rho\\ -i\sigma^\rho & \mathbb{1}\end{pmatrix}\begin{pmatrix}\Psi^j_\uparrow\\ \Psi^j_\downarrow\end{pmatrix}=0, \tag{59}$$

where we set $\rho=R$ and defined

$$\sigma^\rho=\sigma_1\cos\varphi+\sigma_2\sin\varphi. \tag{60}$$

The 4-spinor solutions satisfying these conditions should involve both $\lambda=\pm1/2$ helicities [10],

$$\begin{aligned}\Psi^{\mathrm{edge}}_j\equiv\Psi^{\mathrm{edge}}_{j,\mathrm{MIT}} &= \sum_{\lambda=\pm}C^\lambda_j\check{\Psi}^{\mathrm{edge}}_{j,\lambda}\\ &\equiv\begin{pmatrix}(E^{\mathrm{edge}}_j+M)(C^+_j\check{\phi}^+_j+C^-_j\check{\phi}^-_j)\\ p_j(C^+_j\check{\phi}^+_j-C^-_j\check{\phi}^-_j)\end{pmatrix},\end{aligned} \tag{61}$$

because the MIT boundary condition (9) breaks the helicity conservation.

The self-consistency requirement for the MIT condition (59) and (61) gives us the relation (38) which determines the value of ν_m.

From Eq. (38), it follows that the nontrivial solutions for $\nu=\nu_m$ exist if and only if $M<0$. Solving Eq. (38) as a quadratic equation, we get

$$\begin{aligned} i_m\equiv\frac{I_{m+1}(\nu_m)}{I_m(\nu_m)} &= -\frac{MR+\mathrm{sign}(\mu_m)M^{\mathrm{edge}}_m R}{\nu_m}\\ &\equiv\begin{cases}-\frac{MR+M^{\mathrm{edge}}_m R}{\nu_m}, & m\geq 0,\\ -\frac{MR-M^{\mathrm{edge}}_m R}{\nu_m}, & m<0,\end{cases}\end{aligned} \tag{62}$$

where the angular momentum μ_m and the mass of the edge state M^{edge}_m are given in Eqs. (17) and (44), respectively.

The coefficients in Eq. (61) satisfy the relation

$$\sum_{\lambda=\pm1/2}C^\lambda_j(1+2\lambda\kappa_j)=0, \tag{63}$$

where

$$\kappa_j = \frac{p_j(E_j^{\rm edge} + M + \nu_m i_m/R)}{k[E_j^{\rm edge} + M]} = \frac{p_j(E_j^{\rm edge} - {\rm sign}(\mu_m) M_m^{\rm edge})}{k(E_j^{\rm edge} + M)} \equiv \frac{k(E_j^{\rm edge} - M)}{p_j(E_j^{\rm edge} + {\rm sign}(\mu_m) M_m^{\rm edge})}, \tag{64}$$

and we adopted the usual convention $C_j^{\pm 1/2} \equiv C_j^{\pm}$. One can also rewrite the last expression in the following explicit form:

$$\kappa_j = \frac{p_j(\sqrt{k^2 + M^2 - \frac{\nu_m^2}{R^2}} - {\rm sign}(\mu_m)\sqrt{M^2 - \frac{\nu_m^2}{R^2}})}{k(\sqrt{k^2 + M^2 - \frac{\nu_m^2}{R^2}} + M)}.$$

Combining (63) and (61), we get the edge eigenmode in the explicit form:

$$\Psi_j = C_0^j \begin{pmatrix} (E_j^{\rm edge} + M)(\kappa_j k - p_j) e^{im\varphi} I_m(\nu_m \frac{\rho}{R}) \\ \frac{\nu_m}{iR}(E_j^{\rm edge} + M)\kappa_j e^{i(m+1)\varphi} I_{m+1}(\nu_m \frac{\rho}{R}) \\ p_j(p_j\kappa_j - k) e^{im\varphi} I_m(\nu_m \frac{\rho}{R}) \\ i p_j \frac{\nu_m}{R} e^{i(m+1)\varphi} I_{m+1}(\nu_m \frac{\rho}{R}) \end{pmatrix}. \tag{65}$$

The overall constant C_0^j is determined by the orthonormalization condition given in Eq. (29). For the edge mode, the Dirac inner product is given by

$$\begin{aligned} \langle U_j^{\rm edge}, U_{j'}^{\rm edge}\rangle = {} & \delta(k-k')\delta_{mm'}\theta(E_j^{\rm edge}E_{j'}^{\rm edge})|C_0|^2 \\ & \times \left[\left\{(E_j^{\rm edge}+M)^2(\kappa_j k - p_j)^2 + p_j^2(p\kappa_j - k)^2 + \left(\frac{\nu_m^2}{R^2}(E_j^{\rm edge}+M)^2\kappa_j^2 + p_j^2\frac{\nu_m^2}{R^2}\right)\right\}\mathcal{I}^+_{m+1/2}\right. \\ & \left. + \left\{(E_j^{\rm edge}+M)^2(\kappa_j k - p)^2 + p^2(p\kappa_j - k)^2 - \left(\frac{\nu_m^2}{R^2}(E_j^{\rm edge}+M)^2\kappa_m^2 + p_j^2\frac{\nu_m^2}{R^2}\right)\right\}\mathcal{I}^-_{m+1/2}\right], \end{aligned} \tag{66}$$

where $\mathcal{I}^{\pm}_{m+1/2}$ is defined as

$$\begin{aligned} \mathcal{I}^+_{m+1/2}(\nu_m) &= \int_0^R d\rho\rho \frac{I_m^2(\nu_m\frac{\rho}{R}) + I_{m+1}^2(\nu_m\frac{\rho}{R})}{2} = \frac{R^2}{2}\frac{1}{\nu_m} I_m(\nu_m) I_{m+1}(\nu_m), \\ \mathcal{I}^-_{m+1/2}(\nu_m) &= \int_0^R d\rho\rho \frac{I_m^2(\nu_m\frac{\rho}{R}) - I_{m+1}^2(\nu_m\frac{\rho}{R})}{2} = \frac{R^2}{2}\left[I_m^2(\nu_m) - \frac{2m+1}{\nu_m} I_m(\nu_m) I_{m+1}(\nu_m) - I_{m+1}^2(\nu_m)\right]. \end{aligned} \tag{67}$$

Thus, the normalization coefficient C_0^j is given by the following expression:

$$\begin{aligned} C_0^j = \frac{1}{|I_m(\nu_m)|}\frac{\sqrt{2}k}{p_j\sqrt{\nu_m}} & \left[\left[\left\{k^2 + (E_j^{\rm edge} - M)^2 + \frac{\nu_m^2}{R^2}\right\} i_m^2 + 4\frac{\nu_m M}{R} i_m + \left\{k^2 + (E_j^{\rm edge}+M)^2 + \frac{\nu_m^2}{R^2}\right\}\right] i_m \right. \\ & \left. + \left[2E_j^{\rm edge}(E_j^{\rm edge} - M) i_m^2 - 4\frac{\nu_m E}{R} i_m - 2E_j^{\rm edge}(E_j^{\rm edge} + M)\right]\left(1 - \frac{2m+1}{\nu_m} i_m - i_m^2\right)\right]^{-1/2}. \end{aligned} \tag{68}$$

In the special case $k = 0$, one gets the following explicit expression of the edge eigenmode:

$$\Psi_j = C_0^j \begin{pmatrix} \theta(\mu_m)(M + M_m^{\rm edge}) e^{im\varphi} I_m(\frac{\nu_m\rho}{R}) \\ \theta(-\mu_m)(M + M_m^{\rm edge}) e^{i(m+1)\varphi} I_{m+1}(\frac{\nu_m\rho}{R}) \\ -i\nu_m\theta(-\mu_m) e^{im\varphi} I_m(\frac{\nu_m\rho}{R}) \\ -i\nu_m\theta(\mu_m) e^{i(m+1)\varphi} I_{m+1}(\frac{\nu_m\rho}{R}) \end{pmatrix}. \tag{69}$$

The normalization coefficient (for $m \geq 0$ so far) is given by the expression

$$C_0^j = \frac{1}{|I_m(\nu_m)|}\cdot(\gamma_m[\nu_m + 2m\gamma_m M_m^{\rm edge} - 2\gamma_m(M_m^{\rm edge})^2])^{-\frac{1}{2}}, \tag{70}$$

where

$$\gamma_m = -\frac{(M + M^{\rm edge})R}{\nu_m}. \tag{71}$$

Notice that $0 < \gamma_m < 1$.

The solutions (65) correspond to the edge modes because their density $\bar\psi\gamma^0\psi \equiv \psi^\dagger\psi$ grows exponentially as one approaches the edge of the cylinder at $\rho = R$, Fig. 3. We

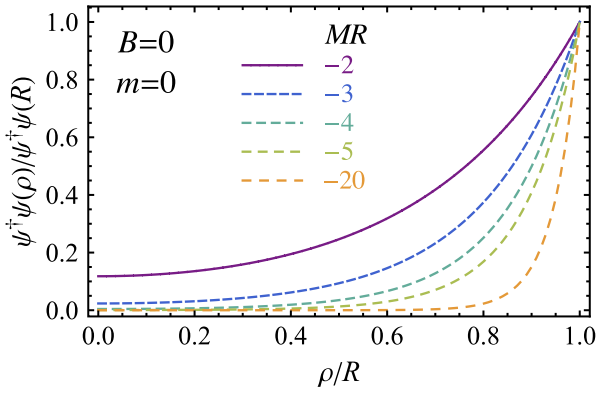

FIG. 3. An example of the density of the edge modes for $k = 0$ and $m = 0$ at various fermionic masses M in the absence of the background magnetic field ($B = 0$). For the sake of convenience, in this figure, we show the density normalized to unity at $\rho = R$.

see that the higher the absolute value of the (negative) fermion mass M, the stronger the localization of the edge modes at the cylinder's boundary. Since all modified Bessel functions I_n grow exponentially at large values of its argument, the localization length of the edge states (65) at the boundary of the cylinder is determined by the length scale

$$\xi_m^{\text{edge}} = \frac{R}{\nu_m}. \tag{72}$$

Thus, the edge modes are characterized by two dimensionful parameters, their mass (44), and the localization length (72). Notice that the former may be expressed via the latter:

$$M_m^{\text{edge}} = \sqrt{M^2 - (\xi_m^{\text{edge}})^{-2}}. \tag{73}$$

Now, let us consider the behavior of the masses of the edge modes M^{edge} in the limit of a large negative fermion mass M. For a large positive real $z \gg 1$, the modified Bessel functions have the following asymptotic expansion:

$$I_m(z) = \frac{e^z}{\sqrt{2\pi z}}\left(1 + \frac{1-4m^2}{8z} + O(z^{-2})\right). \tag{74}$$

Substituting Eq. (74) into the relation (62), we get that in the limit of a large negative mass M the solutions ν^{edge} behave as

$$\nu_m^{\text{edge}} = |M|R - \frac{\mu_m^2}{2|M|R} + O((MR)^{-2}), \tag{75}$$

where μ_m is the total angular momentum of the mode (17).

Therefore, in the limit of the infinite fermionic mass, the masses of the edge modes remain finite, contrary to the bulk modes M_{ml}^{bulk} which become infinitely massive in this limit (32) and therefore decouple from the system. Moreover, in the limit of large (negative) fermion mass, the mass spectrum of the edge modes may be computed analytically:

$$M_{\infty,m}^{\text{edge}} = \lim_{M\to-\infty} M_m^{\text{edge}} = \frac{|\mu_m|}{R}. \tag{76}$$

We find that the masses of the edge modes (76) are (i) finite and (ii) quantized. According to Eq. (75), the localization length (72) tends to zero in this limit. The edge states are double-degenerate as the modes with opposite angular momenta (μ_m and $\mu_{-1-m} \equiv -\mu_m$) possess the same mass. We also stress that in the absence of magnetic field there are no massless edge modes in the spectrum in a cylinder of a finite radius R. The modes eventually become massless in the limit of a large radius $R \to \infty$.

We would like to stress that in this section we discuss the edge eigenmodes, which are characterized by purely imaginary solutions $q_m = i\nu_m$ of the eigenvalue Eq. (27), as contrasted to real solutions q_m of the "bulk" states found in Ref. [10] and discussed in Sec. II B above. The components of the spinor wave functions of the edge eigenmodes (65) are proportional to the modified Bessel functions I_m, which, in turn, satisfy the asymptotic expansion (74). This implies that the density of a zero mode ψ for any angular momentum m behaves as $\psi^\dagger\psi \sim e^{2|M|(\rho-R)}$ in the limit of large (negative) fermion mass $|M|$. Thus, the density of a typical edge mode becomes the exponentially increasing function as the distance at the radial coordinate approaches the edge of the cylinder, $\rho = R$. In a contrast, the density of a typical bulk mode with real q_m is localized in the bulk of the system, as demonstrated in Fig. 4. The larger the excitation number l of the bulk state, the more its density gets concentrated to the center of the cylinder. Therefore, we choose the name "edge mode" for the whole family of purely imaginary solutions $q_m = i\nu_m$ despite that for low values of the fermion mass $|M|$ this family of solutions has a nonzero density in the middle of the cylinder, Fig. 3.

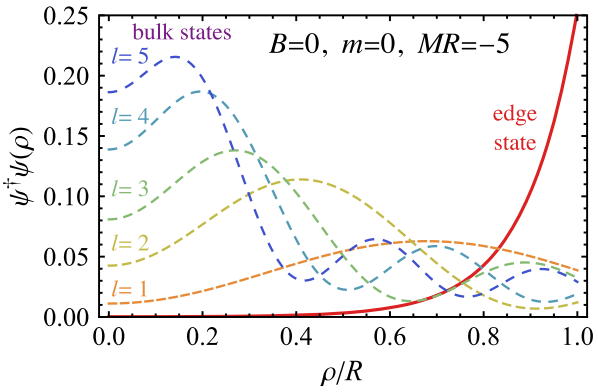

FIG. 4. Five lowest bulk states (the dashed lines) and the edge mode (the solid line) for $MR = -5$ and $m = 0$ at zero magnetic field. The modes are normalized according to Eq. (30).

In conclusion of this section, we would like to notice that the physical particle-antiparticle interpretation of the fermionic modes in the second-quantization formalism depends on the presence of the modes for which $E_j\tilde{E}_j < 0$. The physical meaning of such modes is ambiguous (see Refs. [4,7] as well as the detailed discussion in Ref. [10]), and therefore the absence of such modes in the spectrum makes the theory well defined. In short, the modes $E_j > 0$ ($E_j < 0$) in the laboratory frame are interpreted as particle (antiparticle) states in the Vilenkin quantization [4], while the modes with $\tilde{E}_j > 0$ ($\tilde{E}_j < 0$) in the corotating frame are interpreted as particle (antiparticle) states in the quantization of Iyer [7]. Both vacua are the same, provided $E_j\tilde{E}_j > 0$ for all modes. In Ref. [10], it was indeed found that for uniformly rotating states bounded within the light cylinder (so that with $|\Omega|R < 1$) with physically reasonable boundary conditions the condition $E_j\tilde{E}_j > 0$ is satisfied for all bulk modes [10] so that the rotating (Iyer) and laboratory (Vilenkin) vacua are equivalent. Below, we show that the same identity is also true for the edge modes,

$$E_j^{\rm edge}\tilde{E}_j^{\rm edge} > 0, \tag{77}$$

provided they rotate within the light cylinder, $|\Omega|R < 1$.

Since the energy for $k \neq 0$ is grater than the one for $k = 0$, we focus on the energy for $k = 0$,

$$|E_j^{\rm edge}| = M_m^{\rm edge}. \tag{78}$$

The derivative of $E_m^{\rm edge}$ with respect to M is given by

$$\frac{d|E_j^{\rm edge}|}{dM} = \frac{M - \frac{\nu_m}{R^2}\frac{d\nu_m}{dM}}{|E_j^{\rm edge}|}. \tag{79}$$

The derivative can be also expressed via Eq. (62),

$$\frac{1}{R}\frac{d\nu_m}{dM}\frac{I_{m+1}(\nu_m)}{I_m(\nu_m)}\left(1 + \nu_m\frac{I'_{m+1}}{I_{m+1}} - \nu_m\frac{I'_m}{I_m}\right) = -1 - {\rm sign}(\mu_m)\frac{d|E_j^{\rm edge}|}{dM}, \tag{80}$$

with $I'_m(\nu_m) = dI_m(\nu_m)/d\nu_m$. Using the properties of the modified Bessel functions,

$$I'_m(z) = \frac{m}{z}I_m(z) + I_{m+1}(z), \tag{81}$$

$$I'_{m+1}(z) = I_m(z) - \frac{m+1}{z}I_{m+1}(z), \tag{82}$$

the derivative can be rewritten as

$$\frac{d|E_j^{\rm edge}|}{dM} = \frac{2|\mu_m|M - 2|E_j^{\rm edge}|MR - |E_j^{\rm edge}|}{2|\mu_m||E_j^{\rm edge}| - 2(E_j^{\rm edge})^2R - M}. \tag{83}$$

If there is a local minimum at $M = M_0 < M_c^{(m)} < 0$, the energy is given by

$$|E_j^{\rm edge}|R = \frac{2M_0R}{1 + 2M_0R}|\mu_m|. \tag{84}$$

Because of the non-negativity of the left-hand side of the above equation, the local minimum can exist only for $M_0R < -1/2$. In this region, the inequality $|E_j^{\rm edge}|R > |\mu_m|$ is satisfied at all local minima, and thus $E_j^{\rm edge}\tilde{E}_j^{\rm edge} > 0$ is satisfied for $\Omega R < 1$ (here, we take for simplicity $\Omega > 0$). There is also a possibility that the minimum is achieved at the ends, $MR \to -|\mu_m| - 1/2$ or $M \to -\infty$. At such points, the energies are given by $E_j^{\rm edge} = (|\mu_m| + 1/2)/R$ and $E_j^{\rm edge} = |\mu_m|/R$, respectively. Therefore, in the region of $MR \in (-\infty, -|\mu_m| - 1/2)$, the relation $E_j^{\rm edge}\tilde{E}_j^{\rm edge} > 0$ is always satisfied for the uniform rotation within the light cylinder $\Omega R < 1$.

III. BULK AND EDGE SOLUTIONS IN THE MAGNETIC FIELD BACKGROUND

In this section, we derive, following the general line of the previous section, the eigenspectrum of the Dirac fermions in the background of magnetic field.

A. Dirac equation in rotating space-time in the uniform magnetic field

In the presence of an external magnetic field parallel to the cylinder axis $\boldsymbol{B} = (0, 0, B_z \equiv B)$, the Dirac Eq. (4) is modified,

$$[i\gamma^\mu(D_\mu + \Gamma_\mu) - M]\psi = 0, \tag{85}$$

where $D_\mu = \partial_\mu - ieA_\mu$ is the covariant derivative. In the laboratory frame, the corresponding gauge field can be chosen in the symmetric form

$$A_{\hat{i}} = \left(0, \frac{By}{2}, -\frac{Bx}{2}, 0\right). \tag{86}$$

In the corotating frame, the background gauge field is as follows:

$$A_\mu = \left(-\frac{B\Omega r^2}{2}, \frac{By}{2}, -\frac{Bx}{2}, 0\right). \tag{87}$$

The Dirac Eq. (85) can be explicitly written as follows:

$$\left[i\gamma^{\hat{t}}\left(\partial_t + y\Omega\partial_x - x\Omega\partial_y - \frac{i}{2}\Omega\sigma^{\hat{x}\hat{y}}\right) + i\gamma^{\hat{x}}\left(\partial_x + \frac{ieBy}{2}\right) + i\gamma^{\hat{y}}\left(\partial_y - \frac{ieBx}{2}\right) + i\gamma^{\hat{z}}\partial_z - M\right]\psi = 0. \tag{88}$$

As in the absence of magnetic field, the eigenvectors of the Dirac Eq. (88) are labeled by the eigenvalues of commuting operators $\{\hat{\tilde{H}}, \hat{P}_z, \hat{J}_z, \hat{W}\}$, where $\hat{\tilde{H}}$ is the corotating Hamiltonian, $\hat{P}_z$ is the z component of the momentum operator, $\hat{J}_z$ is the z component of the total angular momentum (18), and $\hat{W}$ is the helicity operator. In the presence of magnetic field, these operators coincide with the ones given in Sec. II with the substitution $\hat{\boldsymbol{P}} \to \hat{\boldsymbol{P}} + e\hat{\boldsymbol{A}}$, which accounts for the gauge invariance of these operators. In the presence of magnetic field, the corotating energy $\tilde{E}_j$ is related to the laboratory energy E_j according to Eq. (16).

Notice that Eq. (88) is gauge invariant because of the identity which holds for usual ∂_μ and covariant D_μ derivatives in the corotating reference frame:

$$\partial_t + y\Omega\partial_x - x\Omega\partial_y \equiv D_t + y\Omega D_x - x\Omega D_y. \quad (89)$$

Here, we used the fact that in the rotating frame the gauge field (87) acquires the compensating time component $A_0 = -B\Omega r^2/2$.

In fact, relation (89) has a much deeper sense than just a simple mathematical identity. In the absence of the magnetic background, the relation between the energies in corotating and laboratory frames is given by Eq. (16). Since thermodynamical and mechanical properties of the system depend on the energies in the corotating (rather then laboratory) frame, it is important to figure out if the relation (16) still holds in the presence of magnetic field B or not. Indeed, to maintain the gauge invariance, the usual derivatives ∂_μ in the presence of magnetic field in all physical operators should transform to the covariant derivatives $D_\mu = \partial_\mu - ieA_\mu$. In particular, the angular momentum operator (18) should become

$$\hat{J}_z(A) = J_z - ieA_\varphi \equiv -i\partial_\varphi + \frac{1}{2}\Sigma_z - \frac{eBr^2}{2}, \quad (90)$$

where $J_z \equiv J_z(A=0)$. Therefore, we could naturally expect that in the presence of magnetic field the crucial corotating-laboratory energy relation (16) could also be modified. To clarify this issue, we notice that the relation (16) comes from the relation between Hamiltonians in the rotating ($\hat{\tilde{H}} = i\partial_t$) and laboratory ($\hat{H} = i\partial_{\hat{t}}$) reference frames,

$$\hat{\tilde{H}} = \hat{H} - \Omega\hat{J}_z, \quad (91)$$

which has been used so far at vanishing magnetic field. However, in the presence of magnetic field, the gauge-covariant Hamiltonian in the corotating frame is given by

$$H = iD_t \equiv i\partial_t + eA_t \quad (92)$$

[while the Hamiltonian in the laboratory frame $\hat{H} \equiv iD_{\hat{t}}$ remains untouched as $A_{\hat{t}} \equiv 0$ according to Eq. (86)] so that the eigenvalue equation for the energy levels becomes

$$iD_t\psi = [\hat{H} - \Omega\hat{J}_z(A)]\psi. \quad (93)$$

However, taking into account in the rotating frame $A_t = \Omega A_\varphi \equiv -B\Omega r^2/2$ [used already in Eq. (89)], we arrive at the conclusion that the "covariantization" of the Hamiltonian (92) and the covariantization of the angular momentum operator (90) exactly cancel each other in Eq. (93), and we arrive at

$$i\partial_t\psi = (\hat{H} - \Omega J_z)\psi. \quad (94)$$

Next, we notice that the energy in the corotating frame enters the wave function as $\psi(t,\boldsymbol{x}) = \exp\{-i\tilde{E}_j t\}\psi(\boldsymbol{x})$, and therefore one gets from Eq. (94)

$$\tilde{E}_j\psi(\boldsymbol{x}) = (\hat{H} - \Omega J_z)\psi(\boldsymbol{x}), \quad (95)$$

which agrees with Eq. (91), which, in turn, leads to the relation in question (16). Thus, we conclude that the relation (16) between the energies in the corotating $\tilde{E}$ and laboratory E frames is still valid in the presence of the magnetic field background.

B. Solutions

A general solution of the Dirac Eq. (88) has the form

$$U_j(t,z,\rho,\varphi) = \frac{1}{2\pi}e^{-i\tilde{E}_j t + ikz}u_j(\rho,\varphi), \quad (96)$$

where u_j is an eigenspinor. The diagonal forms of $\hat{J}_z$ and $\hat{W}$ allow us to express the eigenspinor u_j as

$$u_j^\lambda(\rho,\varphi) = \begin{pmatrix} C_j^{\lambda,\mathrm{up}}\phi_j^\lambda(\rho,\phi) \\ C_j^{\lambda,\mathrm{down}}\phi_j^\lambda(\rho,\phi) \end{pmatrix}, \quad (97)$$

where the 2-spinor

$$\phi_j^\lambda(\rho,\phi) = \begin{pmatrix} e^{im\varphi}\chi_{j-}^\lambda(\rho) \\ e^{i(m+1)\varphi}\chi_{j+}^\lambda(\rho) \end{pmatrix} \quad (98)$$

is defined via two scalar functions $\chi_{j\pm}^\lambda$ of the radial coordinate ρ with a definite helicity eigenvalue λ. The helicity eigenvalue equation, $\hat{W}U_j^\lambda = \lambda U_j^\lambda$, is reduced to the relation

$$\begin{pmatrix} k & \hat{P}_- + e\hat{A}_- \\ \hat{P}_+ + e\hat{A}_+ & -k \end{pmatrix} \frac{\phi_j^\lambda(\rho,\varphi)}{2\sqrt{E_j^2 - M^2}} = \lambda_j \phi_j^\lambda(\rho,\varphi), \tag{99}$$

with $\hat{P}_\pm + e\hat{A}_\pm = -ie^{\pm i\varphi}(\partial_\rho \pm i\rho^{-1}\partial_\varphi \pm eB\rho/2)$. The equations for $\chi^\lambda_{j\pm}$ are written as follows:

$$\left[\partial_\rho^2 + \frac{\partial_\rho}{\rho} - \left(\frac{m+1}{\rho}\right)^2 + meB - \frac{e^2B^2}{4}\rho^2 + (E_j^2 - M^2 - k^2)\right]\chi^\lambda_{j+} = 0, \tag{100}$$

$$\left[\partial_\rho^2 + \frac{\partial_\rho}{\rho} - \left(\frac{m}{\rho}\right)^2 + (m+1)eB - \frac{e^2B^2}{4}\rho^2 + (E_j^2 - M^2 - k^2)\right]\chi^\lambda_{j-} = 0. \tag{101}$$

Using the substitution $\xi \equiv \frac{eB}{2}\rho^2$, the above equations are reduced, respectively, to a simpler set of relations,

$$\xi(\chi^\lambda_{j+})'' + (\chi^\lambda_{j+})' + \left(-\frac{1}{4}\xi + \beta_j^+ - \frac{(m+1)^2}{4\xi}\right)\chi^\lambda_{j+} = 0, \xi(\chi^\lambda_{j-})'' + (\chi^\lambda_{j-})' + \left(-\frac{1}{4}\xi + \beta_j^- - \frac{m^2}{4\xi}\right)\chi^\lambda_{j-} = 0, \tag{102}$$

where

$$\beta_j^\pm = \frac{2\mu_m \mp 1}{4} + \frac{1}{2eB}(E_j^2 - M^2 - k^2) \tag{103}$$

and the angular momentum μ_m is given in Eq. (17).

The normalizable (regular in the origin) solutions are given by the confluent hypergeometric function $\mathcal{M}(a,b;z) \equiv {}_1F_1(a,b;z)$ [13,22],

$$\chi^\lambda_{j+} = \mathcal{N}^\lambda_{j+}\rho^{|m+1|}e^{-\frac{eB}{4}\rho^2}\mathcal{M}_j^+, \tag{104}$$

$$\chi^\lambda_{j-} = \mathcal{N}^\lambda_{j-}\rho^{|m|}e^{-\frac{eB}{4}\rho^2}\mathcal{M}_j^-, \tag{105}$$

where $\mathcal{M}_j^\pm$ is defined as

$$\mathcal{M}_j^+ \equiv \mathcal{M}\left(a_j^+, |m+1|+1, \frac{eB}{2}\rho^2\right), \tag{106}$$

$$\mathcal{M}_j^- \equiv \mathcal{M}\left(a_j^-, |m|+1, \frac{eB}{2}\rho^2\right) \tag{107}$$

and $a_j^\pm$ is defined as

$$a_j^+ = \frac{1}{2}(|m+1| - m + 1) - \frac{1}{2eBR^2}(q_j^B)^2, \tag{108}$$

$$a_j^- = \frac{1}{2}(|m| - m) - \frac{1}{2eBR^2}(q_j^B)^2 \tag{109}$$

with $q_j^B \equiv \sqrt{E_j^2 - M^2 - k^2}R$. The coefficient $\mathcal{N}^\lambda_{j+}$ can be related to the coefficient $\mathcal{N}^\lambda_{j-}$ by a substitution of Eqs. (104) and (105) into the helicity Eq. (99):

$$\mathcal{N}^\lambda_{j+} = \frac{+i(E_j^2 - M^2 - k^2)}{2(k + 2\lambda\sqrt{E_j^2 - M^2})(m+1)}\mathcal{N}^\lambda_{j-}, \quad m \geq 0,$$

$$\mathcal{N}^\lambda_{j+} = \frac{2im}{k + 2\lambda\sqrt{E_j^2 - M^2}}\mathcal{N}^\lambda_{j-}, \quad m < 0. \tag{110}$$

The 2-spinors ϕ_j^λ with the helicity λ are written as

$$\phi_j^\lambda(\rho,\varphi) = \alpha_j^\lambda \begin{pmatrix} f^\lambda_{j-}\mathcal{M}_j^- \\ f^\lambda_{j+}\mathcal{M}_j^+ \end{pmatrix}, \tag{111}$$

where α_j is an overall constant and the 2-spinor $(f^\lambda_{j-} f^\lambda_{j+})^T$ is defined as

$$\begin{pmatrix} f^\lambda_{j-} \\ f^\lambda_{j+} \end{pmatrix} = \begin{cases} \begin{pmatrix} 2(m+1)G_m(\rho,\varphi) \\ 2i\lambda p_j^B(\mathsf{p}_{-\lambda}^B)^2 G_{m+1}(\rho,\varphi) \end{pmatrix}, & m \geq 0, \\ \begin{pmatrix} p_j^B(\mathsf{p}_\lambda^B)^2 G_m(\rho,\varphi) \\ 4i\lambda m G_{m+1}(\rho,\varphi) \end{pmatrix}, & m < 0, \end{cases} \tag{112}$$

with

$$G_m(\rho,\varphi) = e^{im\varphi}\rho^{|m|}e^{-\frac{eB}{4}\rho^2} \tag{113}$$

and

$$\mathsf{p}_\pm^B = \sqrt{1 \pm \frac{k}{p_j^B}}, \qquad p_j^B = \sqrt{E_j^2 - M^2}. \tag{114}$$

Next, we use the Dirac Eq. (88) to determine the constraint between $C_j^{\lambda\text{up}}$ and $C_j^{\lambda\text{down}}$:

$$\begin{pmatrix} E_j - M & -2\lambda\sqrt{E_j^2 - M^2} \\ 2\lambda\sqrt{E_j^2 - M^2} & -E_j - M \end{pmatrix} u_j^\lambda(\rho,\phi) = 0, \tag{115}$$

or

$$C_j^{\lambda,\text{up}} = \frac{\sqrt{E_j + M}}{2\lambda\frac{E_j}{|E_j|}\sqrt{E_j - M}}C_j^{\lambda,\text{down}}. \tag{116}$$

Consequently, the spinor u_j^λ with the helicity λ can be written as

$$u_j^\lambda(\rho,\varphi) = C_j^\lambda \begin{pmatrix} \mathsf{E}_+ \phi_j^\lambda \\ 2\lambda \frac{E_j}{|E_j|} \mathsf{E}_- \phi_j^\lambda \end{pmatrix} \tag{117}$$

with $\mathsf{E}_\pm = \sqrt{1 \pm \frac{M}{E_j}}$ and an overall constant C_j^λ, which is determined by an orthogonal condition. Notice that the prefactor α_j^λ in Eq. (111) is absorbed into C_j^λ.

The spinor u_j which satisfies the MIT boundary condition (9) can be constructed in terms of the linear combination

$$u_j(\rho,\varphi) = b_j^+ u_j^+(\rho,\varphi) + b_j^- u_j^-(\rho,\varphi). \tag{118}$$

Substituting the eigenmode (96) and (118) into the boundary condition (9) as $\psi \equiv U_j$ and using the explicit form of the eigenspinors (117), we get a matrix equation for the coefficients $b^\pm$ with the solution (118),

$$\mathsf{E}_+(b_j^+\phi_j^+ + b_j^-\phi_j^-)|_{\rho=R} = -\frac{iE_j}{|E_j|}\mathsf{E}_-(b_j^+\sigma^\rho\phi_j^+ - b_j^-\sigma^\rho\phi_j^-)|_{\rho=R}, \tag{119}$$

where σ^ρ is given in Eq. (60). The matrix Eq. (119) can also be represented in the form

$$\begin{pmatrix} i\frac{E_j}{|E_j|}\mathsf{E}_- e^{-i\varphi} f_{j+}^+ \mathcal{M}_j^+ + \mathsf{E}_+ f_{j-}^+ \mathcal{M}_j^- & -i\frac{E_j}{|E_j|}\mathsf{E}_- e^{-i\varphi} f_{j+}^- \mathcal{M}_j^+ + \mathsf{E}_+ f_{j-}^- \mathcal{M}_j^- \\ i\frac{E_j}{|E_j|}\mathsf{E}_- e^{i\varphi} f_{j-}^+ \mathcal{M}_j^- + \mathsf{E}_+ f_{j+}^+ \mathcal{M}_j^+ & -i\frac{E_j}{|E_j|}\mathsf{E}_- e^{i\varphi} f_{j-}^- \mathcal{M}_j^- + \mathsf{E}_+ f_{j+}^- \mathcal{M}_j^+ \end{pmatrix} \begin{pmatrix} b_j^+ \\ b_j^- \end{pmatrix}|_{\rho=R} = 0. \tag{120}$$

We find that Eq. (120) has a nontrivial solution for $b_j^\pm$ if the quantity

$$q_j^B = \sqrt{E_j^2 - M^2 - k^2}R \tag{121}$$

satisfies the relation

$$\begin{cases} (q_j^B)^2(\mathcal{M}_R^+)^2 - 4(m+1)MR\mathcal{M}_R^-\mathcal{M}_R^+ - 4(m+1)^2(\mathcal{M}_R^-)^2 = 0, & m \geq 0, \\ (q_j^B)^2(\mathcal{M}_R^-)^2 - 4mMR\mathcal{M}_R^-\mathcal{M}_R^+ - 4m^2(\mathcal{M}_R^+)^2 = 0, & m < 0, \end{cases} \tag{122}$$

where

$$\mathcal{M}_R^+ \equiv \mathcal{M}_j^+|_{\rho=R} = \mathcal{M}(a_j^+, |m+1|+1, \phi_B/\phi_0),$$
$$\mathcal{M}_R^- \equiv \mathcal{M}_j^-|_{\rho=R} = \mathcal{M}(a_j^-, |m|+1, \phi_B/\phi_0). \tag{123}$$

The magnetic field enters the spectrum in terms of the ratio,

$$\frac{\phi_B}{\phi_0} \equiv \frac{eBR^2}{2}, \tag{124}$$

of the magnetic flux the cross section of the cylinder,

$$\phi_B = \pi BR^2, \tag{125}$$

and the elementary magnetic flux,

$$\phi_0 = \frac{2\pi}{e} \tag{126}$$

(we remind the reader that in our units $\hbar = 1$).

Since the dimensionless quantity q_j^B is obtained by the equation only associated with the angular number m and is discretized in accordance with effects of the boundary condition, it can be labeled by m and the root number $l = 1, 2, 3, \ldots$, i.e. q_{ml}^B.

The zero solutions of Eq. (122), $q_{ml}^B = 0$, are achieved at specific values of the fermion masses $M = M_c^{(m)}$ with

$$M_c^{(m)} = \begin{cases} -\frac{m+1}{R}\frac{1}{\mathcal{M}(1,m+2,\phi_B/\phi_0)}, & m \geq 0, \\ \frac{m}{R}\frac{e^{\phi_B/\phi_0}}{\mathcal{M}(-m,-m+1,\phi_B/\phi_0)}, & m < 0, \end{cases} \tag{127}$$

where we used the properties $\mathcal{M}(0,b,z) = 1$ and $\mathcal{M}(a,a,z) = e^z$. In the limit of vanishing magnetic field, $eB \to 0$, we can recover the result (34) for $M_c^{(m)}$ using the property $\mathcal{M}(a,b,z) = 1 + O(z)$ valid for $z \to 0$. In the limit of strong magnetic field, $eB \to \infty$, the mass becomes

$$M_c^{(m)} = \begin{cases} -\frac{e^{-\phi_B/\phi_0}(\phi_B/\phi_0)^{m+1}}{Rm!} \to 0, & m \geq 0, \\ -\frac{1}{R}\frac{\phi_B}{\phi_0} \to -\infty, & m < 0, \end{cases} \tag{128}$$

where we used the asymptotic expansion $\mathcal{M}(a,b,z) \sim (\Gamma(b)/\Gamma(a))e^z z^{a-b}$ valid at $z \to \infty$ for all values of a except for nonpositive integer a.

We can recover Eq. (27) from Eqs. (122) and (123) in the limit of vanishing magnetic field $eB \to 0$ using the relations (valid for $q_j^B \neq 0$ and $n \geq 0$)

$$a_j^{\pm} \overset{eB\to 0}{\to} -\frac{(q_j^B)^2}{2eBR^2}, \tag{129}$$

$$\lim_{x\to 0} {}_1F_1\left(-\frac{y^2}{2x}, n+1; \frac{x}{2}\right) = n!\left(\frac{2}{y}\right)^n J_n(y), \tag{130}$$

and $J_{-m}(x) = (-1)^m J_m(x)$.

The masses of the bulk and the edge states are given by the same formulas (32) and (44), respectively, as in the case of the $B = 0$ states (with the obvious change $q_{ml} \to q_{ml}^B$). The quantity ν_m^B for the edge states in the background of magnetic field is defined similarly to the $B = 0$ definition in Eq. (37):

$$q_m^B = i\nu_m^B. \tag{131}$$

In the limit of infinitely large fermion mass, $M \to -\infty$, the wave function of the edge mode may be written in an explicit form; see Eq. (145) below.

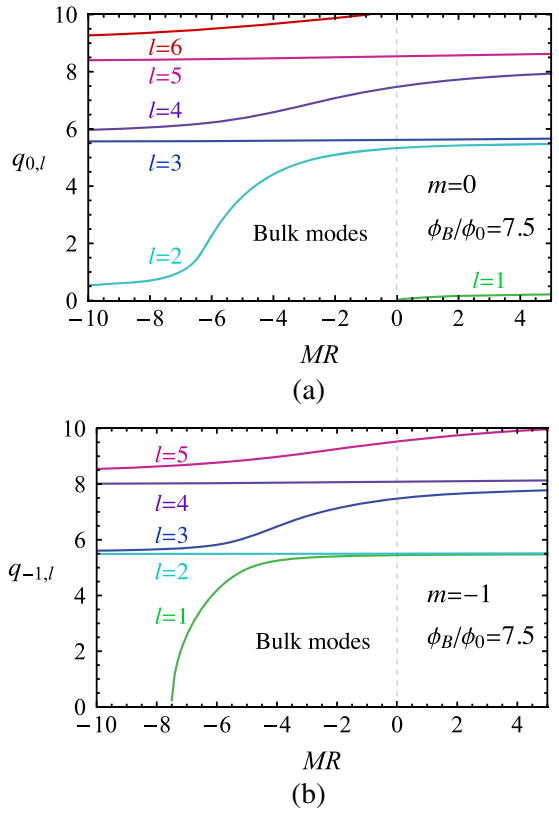

FIG. 5. The bulk q_{ml}^B solutions of Eqs. (122) and (123) vs the fermion mass M in the background of magnetic flux (124) $\phi_B = 7.5\phi_0$ for (a) $m = 0$ and (b) $m = -1$ orbital numbers and various radial excitation numbers l.

C. Properties of the solutions

To obtain the spectrum of free fermions in the cylinder in the presence of external magnetic field, we solve Eqs. (122) and (123) numerically.

In Figs. 5 and 6, we show the behavior of, respectively, the bulk solutions q_{ml}^B and the edge solutions ν_m^B for the orbital angular momentum $m = 0$ (which represents the qualitative behavior of all $\mu_m > 0$ modes) and $m = -1$ (which characterizes general properties of the solutions with $\mu_m < 0$) at nonzero magnetic field. These quantities at zero magnetic field are shown in Fig. 1.

We notice the following effects of background magnetic field on the bulk modes:

(i) *Critical mass.*—At zero magnetic field, the ground states ($l = 1$) disappear at the quantized critical masses $M_c^{(m)}$ given in Eq. (34). As the magnetic field becomes stronger, the critical masses $M_c^{(m)}$ deviate from their $B = 0$ values; for $eB > 0$, the critical masses for the modes with a positive angular momentum $\mu_m > 0$ tend to zero, $M_c^{(m)} \to 0$, while the critical masses of the $\mu_m < 0$ modes tend to negative infinity, $M_c^{(m)} \to -(\phi_B/\phi_0)/R$. The behaviors are consistent with the analytical results given in Eq. (128). One can show that at $eB < 0$ the modes

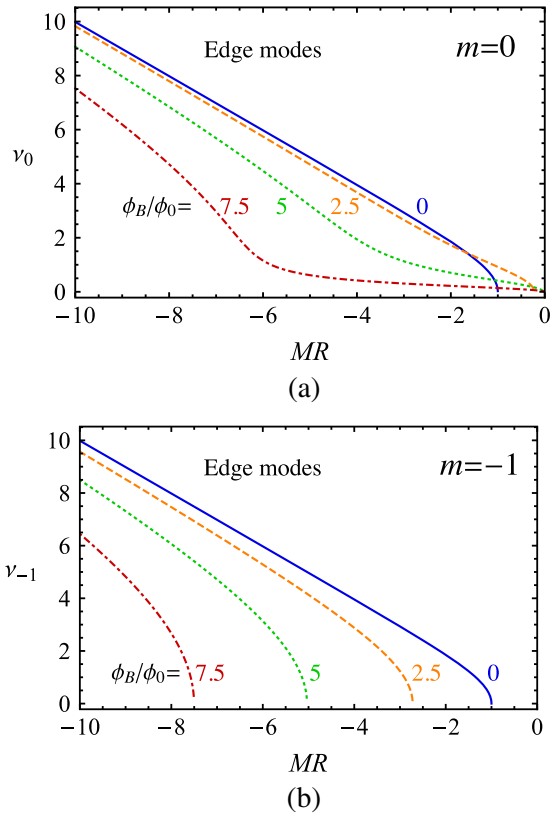

FIG. 6. The edge ν_m^B solutions (131) of Eqs. (122) and (123) vs the fermion mass M in the background of different magnetic fluxes (124) ϕ_B for (a) $m = 0$ and (b) $m = -1$ orbital numbers.

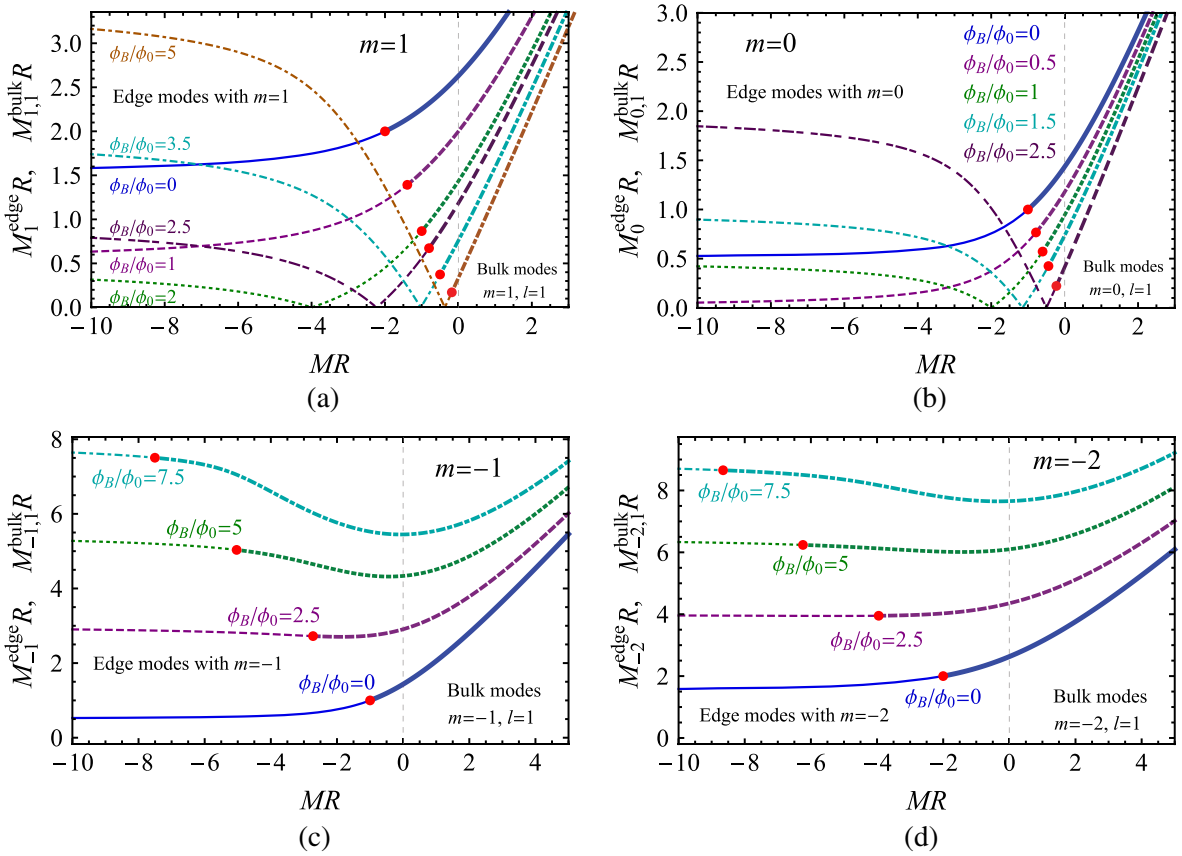

FIG. 7. The masses of the lowest bulk ($l = 1$) and edge states vs the mass of the fermion M for various values orbital angular momenta m and magnetic field B. The bulk (edge) modes are shown by the thicker (thinner) lines, while the positions where the bulk modes are converted to the corresponding edge modes are marked by the red points.

with $\mu_m > 0$ and $\mu_m < 0$ swap their places as $M_c^{(m)} \to -\infty$ for the former and $M_c^{(m)} \to 0$ for the later.

(ii) *Level degeneracy.*—At large positive or negative values of the fermion mass, $M \to \pm\infty$, the levels are grouping into pairs. This is a natural consequence of the growing mass of the bulk levels (32). As the mass become large, the bulk states become more localized in space, and they become less sensitive to the presence of the boundary of the cylinder. Then, the energy spectrum shares a natural similarity with the Landau levels in a boundless space where the spin-up and spin-down states of the excited levels are double degenerate in energy.

The behavior of the edge modes ν_m^B at values of magnetic field—or, equivalently, the magnetic flux ϕ_B, Eq. (125)—is shown in Fig. 6. The mentioned properties of the critical mass are quite consistent with the ones for the bulk modes, as expected. As the fermion mass M decreases, the quantities ν_m become linear functions of the mass M.

In Fig. 7, we show the masses of the lowest ($l = 1$) bulk modes (32) and the edge modes (44) as the functions of the fermion mass M at various values of magnetic field B. We notice the following remarkable properties of these quantities:

(i) Masses for the modes with negative angular momenta μ_m (i.e., with $m = -1, -2, \ldots$) behave regularly as the $l = 1$ bulk modes are transformed into the edge modes at certain critical masses $M = M_c^{(m)}(B)$. These critical masses are growing in absolute value (and negatively valued) functions of magnetic field. At large enough strengths of the background magnetic field, the masses of the bulk modes experience, as functions of the fermion mass M, a global minimum.

(ii) At positive values of the angular momenta μ_m (i.e., at $m = 0, 1, 2, \ldots$), the masses of the edge modes behave rather irregularly. In particular, they vanish at certain mass $M = M_c^{(m)}(B)$,

$$M_m^{\text{edge}}(M_c^{(m)}(B)) = 0, \qquad m \geq 0. \tag{132}$$

In Fig. 8, we plot, for a few values of m, the masses of fermions $M = M_c^{(m)}(B)$ at which the mass of the edge mode become zero (effectively, the massive edge mode becomes the zero mode). These masses are growing (in absolute value) negative-valued functions of the magnetic field B.

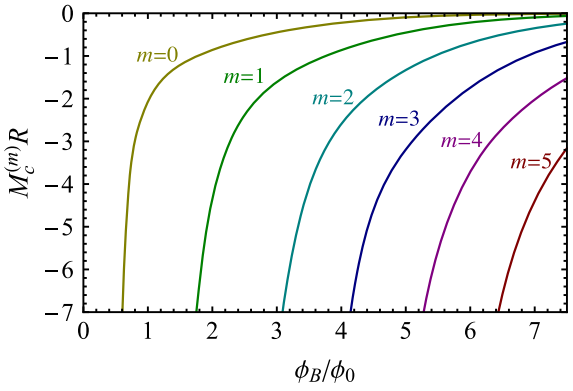

FIG. 8. The values of the fermion masses $M = M_c^{(m)}$ at which the masses of the edge modes vanish (132) vs the magnetic flux ϕ_B for various values of orbital momentum m.

Notice that all these properties are valid for positive magnetic field $eB > 0$. For the negative magnetic field, $eB < 0$, the modes with positive and negative magnetic momenta μ_m swap their places.

As in the absence of magnetic field, in the limit of a large (negative) fermionic mass $M \to -\infty$, the masses of the edge modes remain finite, contrary to the excited $l \geq 2$ bulk modes which become massive (32) and decouple from the system. Moreover, one can check numerically that in this limit the mass spectrum of the edge states fits a simple analytical function:

$$M^{\rm edge}_{\infty,m}(B) = \lim_{M\to-\infty} M^{\rm edge}_m(B) = \left|\mu_m - \frac{\phi_B}{\phi_0}\right| \frac{1}{R}. \qquad (133)$$

In fact, we can obtain the result (133) analytically by using the large a expansion of $\mathcal{M}(a,b,z)$ [23]:

$$\mathcal{M}(a,b,z) = (z/a)^{(1-b)/2} \frac{e^{z/2}\Gamma(1+a-b)\Gamma(b)}{\Gamma(a)} \left[I_{b-1}(2\sqrt{az}) - \sqrt{\frac{z}{a}} I_b(2\sqrt{az}) \left(\frac{b}{2} - \frac{z}{12}\right) + O(a^{-1}) \right]$$
$$= (z/a)^{(1-b)/2} \frac{e^{z/2}\Gamma(1+a-b)\Gamma(b)}{\Gamma(a)} \left[\frac{e^{2\sqrt{az}}}{2\sqrt{\pi\sqrt{az}}} \times \left(1 + \frac{1-4(b-1)^2}{16\sqrt{az}} - \sqrt{\frac{z}{a}} \left(\frac{b}{2} - \frac{z}{12}\right) + O(a^{-1}) \right) \right]. \qquad (134)$$

Substituting Eqs. (134) and (74) into Eq. (122), we obtain the solution of ν_m in terms of the expansion of a large negative mass M,

$$\nu^{\rm edge}_m = |M|R - \frac{(\mu_m - \frac{\phi_B}{\phi_0})^2}{2|M|R} + O((MR)^{-2}), \qquad (135)$$

which leads to Eq. (133).

The masses of the edge states depend on the angular magnetic moment μ_m of the mode and the Aharonov-Bohm phase $\vartheta = \phi_B/\phi_0$. In the limit of vanishing magnetic field, $\phi_B = 0$, Eq. (133) matches with the $B = 0$ result (76). The mass spectrum of the edge states (133) in the $M \to \infty$ limit is shown in Fig. 9.

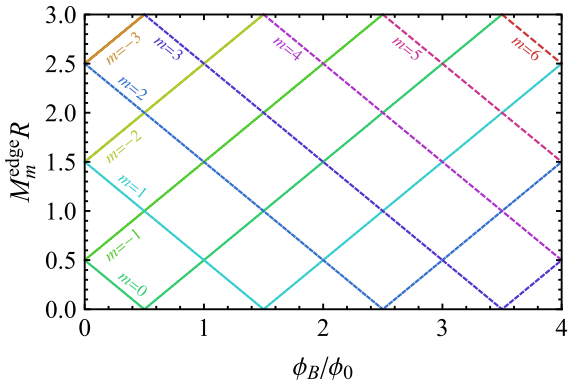

FIG. 9. The masses of the edge modes (76) as functions of magnetic field B in the limit $M \to -\infty$.

IV. EDGE MODES AND ROTATION

A. Zero magnetic field

In the limit of infinite negative mass M, the thermodynamic and rotational properties of the system are determined only by the edge modes. Indeed, the masses of the edge modes remain finite (76), while the masses of the bulk modes tend to infinity, implying that the latter do not contribute to the dynamics of the system. In the absence of magnetic field, the energy of the edge modes (42) is given by the simple expression[2]

$$E^{\rm edge}_j \equiv E^{\rm edge}_m(k_z) = \sqrt{k_z^2 + \frac{\mu_m^2}{R^2}}, \qquad (136)$$

where μ_m is the angular momentum of the edge mode (17) and $m \in \mathbb{Z}$.

The thermodynamic effects of the edge modes are determined by the thermodynamic potential defined in the corotating, as opposed to the laboratory, reference frame (the latter fact is stressed by the tilde sign in $\tilde{F}$):

[2]In this section, we consider only the positively defined branch of the energy eigenmodes $E = +|E|$, which corresponds to the particle edge states (42) both for vanishing (136) and non-vanishing (142) magnetic field.

$$\tilde{F}^{\text{edge}}(T,\Omega) = -\frac{T}{\pi R^2}\sum_{m\in\mathbb{Z}}\int\frac{dk_z}{2\pi} \times [\ln(1+e^{-\frac{E_m^{\text{edge}}(k_z)-\Omega\mu_m}{T}}) + (\Omega\to-\Omega)]. \tag{137}$$

Below, we omit the superscript "edge" in all our notations.

The angular momentum density is given by the derivative of the thermodynamic potential in the corotating reference frame [24]:

$$\boldsymbol{L} = -\left(\frac{\partial\tilde{F}}{\partial\boldsymbol{\Omega}}\right)_T. \tag{138}$$

Since the rotation axis $\boldsymbol{\Omega} = \Omega\mathbf{e}_z$ coincides with the symmetry axis of the cylinder $\mathbf{e}_z$, the angular momentum has only one nonzero component, $\boldsymbol{L} = (0,0,L_z)$.

It is convenient to consider the density of the angular momentum per unit height of the cylinder,

$$\mathcal{L}_z(\Omega) \equiv \pi R^2 L_z(\Omega) = \int_{-\infty}^{\infty}\frac{k_z}{2\pi}\sum_{m\in\mathbb{Z}}\mu_m[f_{m,k_z}(\Omega,T) - f_{m,k_z}(-\Omega,T)], \tag{139}$$

where

$$f_{m,k_z}(\Omega,T) = \frac{1}{e^{\frac{E_m(k_z)-\Omega\mu_m}{T}}+1} \tag{140}$$

is the occupation number of the fermionic edge mode.

The moment of inertia per unit height is related to the density of the angular momentum (139) as follows:

$$\mathcal{I}_z(\Omega) = \frac{\mathcal{L}_z(\Omega)}{\Omega}. \tag{141}$$

The angular momentum (139) and the moment of inertia (141) at zero magnetic field are both shown in Fig. 10. These quantities are, respectively, odd and even functions with respect to the flips of the direction of rotation, $\Omega\to-\Omega$, because the thermodynamic potential (137) is an even function of Ω. Both the angular momentum and the moment of inertia diverge in the ultrarelativistic regime at $\Omega R\to\pm1$. At low temperature, both quantities are weakly dependent on the angular frequency Ω, while in a high-temperature regime, both quantities are In functions of Ω.

In Fig. 11, we show the density of the moment of inertia at zero angular momentum. The moment of inertia is a growing function of temperature because as temperature increases the heavier (energetic) modes may participate in rotation of the system.

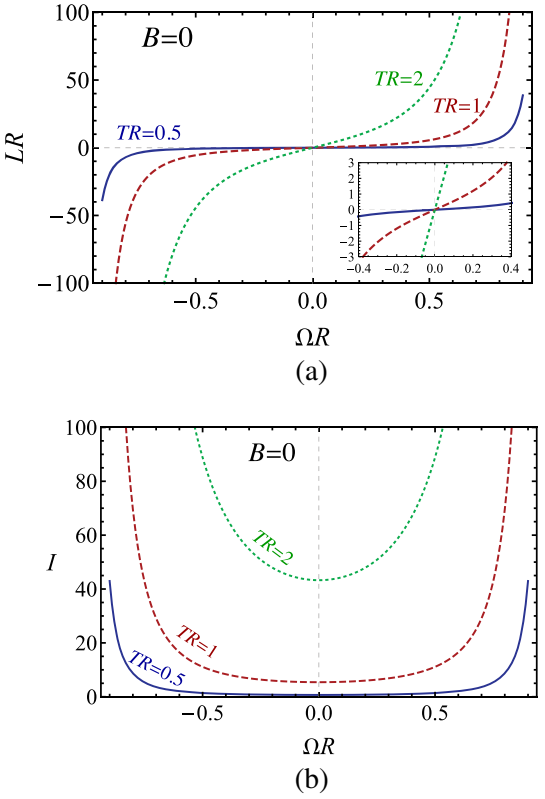

FIG. 10. Densities of (a) the angular momentum (139) and (b) moment of inertia (141) of the cylinder in the limit an infinite fermion mass $M\to\infty$ as the function of angular frequency Ω at various temperatures T and zero magnetic field.

B. Effects of magnetic field

In the presence of magnetic field, the energy dispersion of the edge modes (in the limit of an infinite fermion mass $M\to\infty$) is given by the formula

$$E_m^{\text{edge}}(k_z) = \sqrt{k_z^2 + \frac{1}{R^2}\left(\mu_m - \frac{\phi_B}{\phi_0}\right)^2}, \tag{142}$$

where μ_m is the angular momentum of the edge mode (17) with $m\in\mathbb{Z}$.

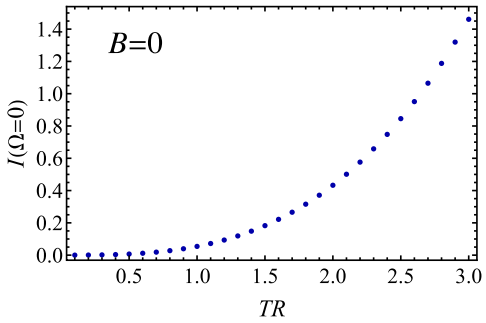

FIG. 11. Density of the moment of inertia (141) at $\Omega=0$ vs temperature T at vanishing magnetic field $B=0$.

The angular momentum (138) can be readily calculated using the partition function (137) and dispersion (142). In Fig. 12, we show the angular momentum L in the magnetic field–angular frequency (B, Ω) plane for temperatures $TR = 0.05,\ 0.1,\ 1$. Naturally, the angular momentum is an increasing function of the angular frequency Ω for every fixed value of magnetic flux ϕ_B and for all temperatures T.

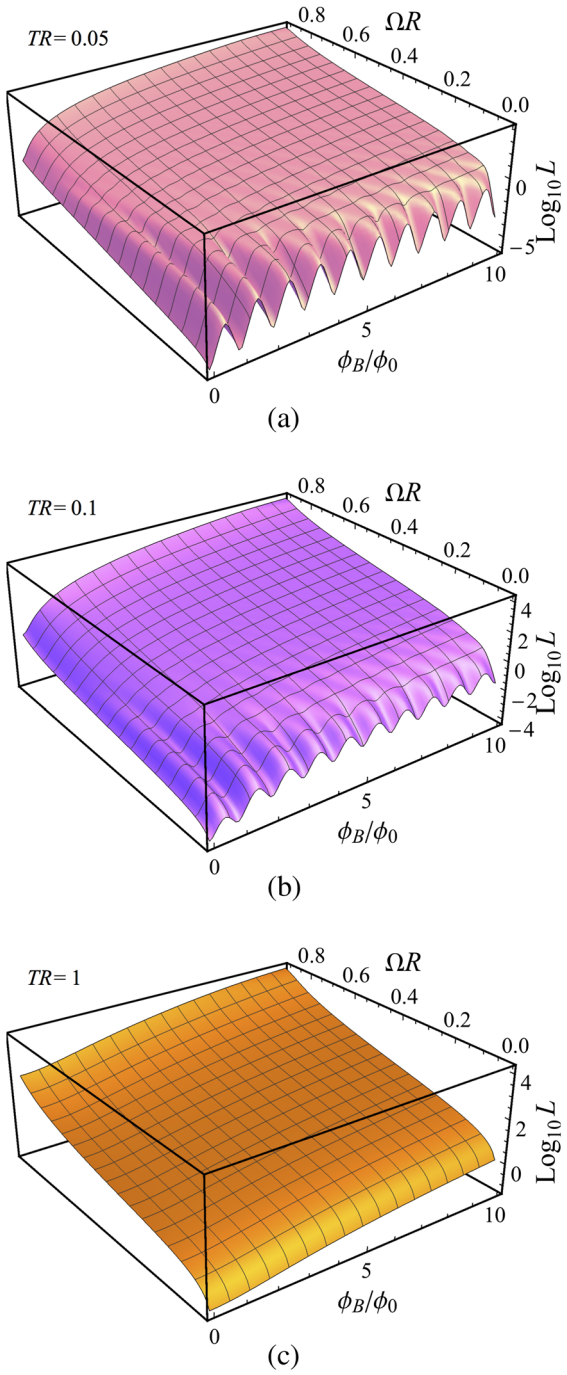

FIG. 12. Angular momentum L of the edge modes per unit height of the cylinder vs the angular frequency Ω and magnetic flux ϕ_B at temperatures $TR = 0.05,\ 0.1,\ 1$ in the limit of infinite fermionic mass $M \to -\infty$ (the bulk modes are absent).

At low temperatures, $TR \lesssim 0.1$, and at slow rotations ($\Omega \sim 10^{-2}/R$), the angular momentum L exhibits oscillating, but nonperiodic, dependence on the value of magnetic flux, as is clearly seen in Figs. 12(a) and 12(b). The local minima and maxima of L approximately correspond to the integer and half-integer values, respectively, of the ratio of magnetic flux ϕ_B and the elementary flux (124). Apart from these oscillations, the value of L slowly increases with the strength of the background magnetic field. This quantum behavior is seen at sufficiently low temperatures; the lower the temperature, the more pronounced oscillations are. There is also a certain small correlation between the magnetic field and the angular frequency seen in the range of middle frequencies, $\Omega R \sim 0.2$.

At higher temperatures $TR \sim 1$, shown in Fig. 12(c), the magnetic-field induced oscillations of the angular momentum disappear completely. At sufficiently fast rotations, the oscillations disappear for all temperatures. In these cases, the angular momentum is an increasing function of both magnetic field B and angular frequency Ω.

In Fig. 13, we show the dependence of the moment of inertia (normalized by the temperature squared) at vanishing angular frequency $\Omega = 0$ vs normalized magnetic flux (124). We clearly see that with the increase of temperature the moment of inertia of the edge modes increases in agreement with zero-field behavior shown in Fig. 11. Similarly to the angular momentum, the moment of inertia experiences (nonperiodic) oscillations as a function of magnetic field. The local minima (maxima) approximately correspond to the integer (half-integer) values of the magnetic flux [calculated in units of the elementary flux (124)]. The oscillatory quantum behavior is pronounced well at low temperatures while at higher temperatures, the dependence of the moment of inertia on the magnetic flux reduces to a monotonically increasing function. These features are also very visible in Fig. 14(a), which shows the moment of inertia I vs both magnetic flux ϕ_B and

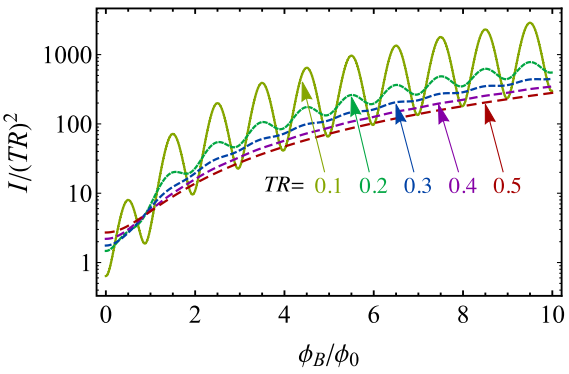

FIG. 13. Moment of inertia (divided by temperature squared) per unit height of the cylinder vs the flux ϕ_B of the background magnetic field at (a) vanishing angular frequency $\Omega = 0$ and (b) nonzero frequency $\Omega R = 0.5$.

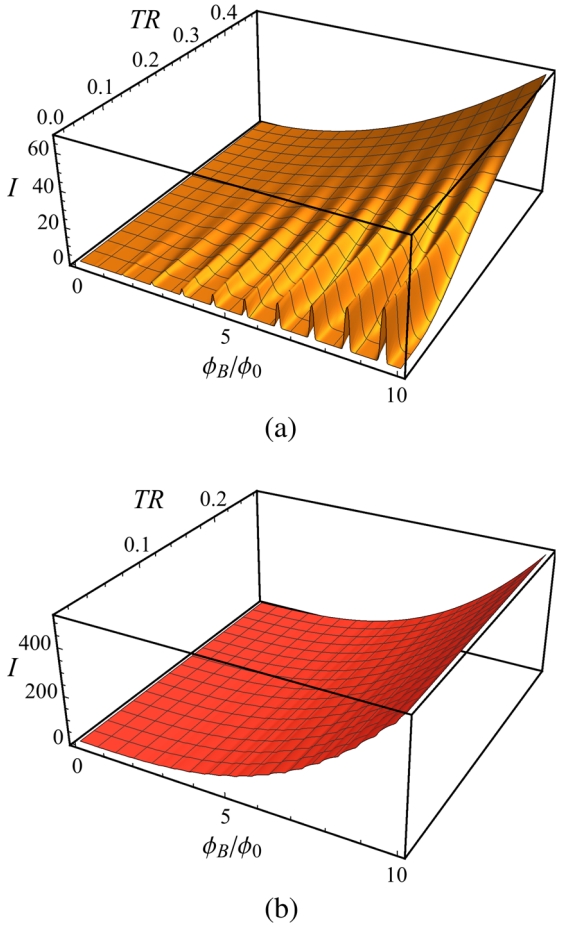

FIG. 14. Moment of inertia per unit height of the cylinder vs magnetic flux ϕ_B and temperature T at (a) vanishing ($\Omega = 0$) and (b) nonzero ($\Omega R = 0.5$) angular frequency.

temperature T at zero frequency $\Omega = 0$. At larger angular frequencies, the oscillations are damped, and the low-temperature behavior of the moment of inertia is similar to the one in its featureless high-temperature region, Fig. 14(b).

The fact that both the moment of inertia and the angular momentum are not a periodic function of magnetic field is a natural consequence of the nonequivalence of magnetic field and rotation in relativistic domain. Indeed, in many nonrelativistic quantum-mechanical applications, a (slow) rotation may be treated as a (weak) magnetic field. This fact is used, for example, in characterizing the spectrum of rotation optical lattices of cold atoms [25]. The equivalence is no more true in the case of a fast relativistic rotation; the effects of rotation and magnetic field in this case are very different [13,15]. To highlight the difference between rotation and magnetic field, we mention that the ground-state degeneracy is independent of the value of the angular frequency, contrary to case of magnetic field [15]. Moreover, the phenomenon of dimensional reduction, which govern many interesting effects in magnetic field background, does not exist in the case of rotation [15].

C. Anomalous transport properties of edge modes

As we mentioned in the Introduction, the quantum field theories may exhibit anomalous transport associated with quantum anomalies that break otherwise conserved classical symmetries of the theory (for details, we refer to Ref. [26] for reviews). In particular, in theories with chiral fermions, the axial anomaly leads to a family of transport phenomena of which the best known representatives are the chiral vortical effect [3] and the chiral magnetic effect [27]. In general, the anomalous chiral effects generate steady electric (vector) and chiral (axial) currents of chiral fermions in the rotating fermionic medium and/or in the background of magnetic field. These effects are realized at finite density and/or in a chirally imbalanced medium with different numbers of left-handed and right-handed chiral fermions. The chiral nature of fermions is essential for these processes as the chiral fermionic number is a conserved quantity for massless (chiral) fermions. Therefore, the anomalous transport phenomena are predominantly discussed in the scope of theories possessing relativistic massless fermions.

Coming back to our case of massive Dirac fermions in the cylinder, we notice that, even in the case of massive bulk fermions, the edge modes may become massless states for certain quantized values of background magnetic field B_c. In particular, for the case of the infinitely massive bulk fermions, $M \to \infty$, the masses of the light edge states vanish for half-integer fluxes ϕ_B of magnetic field (cf. Fig. 9):

$$\phi_{B_c} = \left(n + \frac{1}{2}\right)\phi_0, \qquad n \in \mathbb{Z}. \tag{143}$$

With the help of Eqs. (124), (125), and (126), this condition may be rewritten as follows:

$$B_c = \frac{2n+1}{eR^2}, \qquad n \in \mathbb{Z}. \tag{144}$$

At the critical magnetic field (144), the energy spectrum of edge modes (142) contains a mode with the linear dispersion: $E_m^{\text{edge}} = |k_z|$

Since at the critical values of magnetic field (144) the mass of the edge mode vanishes, one could expect that the anomalous chiral phenomena may be realized via the massless edge modes even for the infinitely massive bulk fermions. To check this hypothesis, we explicitly write the wave functions of the edge modes in the limit $M \to -\infty$,

$$\Psi_m^{\rm edge} = \frac{1}{2\pi R^2}\sqrt{\frac{|M|}{2E_m(E_m R-\mu_m+\frac{\phi_B}{\phi_0})}}e^{-i\tilde{E}_m t+ik_z z} \cdot \begin{pmatrix} k_z R e^{im\varphi} \\ -i(E_m R-\mu_m+\frac{\phi_B}{\phi_0})e^{i(m+1)\varphi} \\ (E_m R-\mu_m+\frac{\phi_B}{\phi_0})e^{im\varphi} \\ ik_z R e^{i(m+1)\varphi} \end{pmatrix} e^{|M|(\rho-R)}, \quad (145)$$

where the energy of the edge mode $E_m \equiv E_m^{\rm edge}$ is given in Eq. (142) and $\tilde{E}_m = E_m - \Omega\mu_m$ according to Eq. (45). The solution (145) may be explicitly derived following all steps of Sec. III B in the simplifying limit $M \to -\infty$.

Using the explicit form of the eigenfunction (145), we find that, despite that the mass of the edge mode vanishes at the critical magnetic field (144), the eigenmode itself is not chiral at any value of the magnetic flux[3]:

$$\gamma^5\Psi_m^{\rm edge} \neq \pm\Psi_m^{\rm edge}. \quad (146)$$

This property is consistent with the fact that the edge modes do not possess a definite helicity, Sec. II C.

Therefore, we come to a conclusion that one cannot define left-handed and right-handed chiral edge modes and, consequently, the chirally imbalanced edge matter is not a well-defined physical notion. As a result, one may expect that the anomalous transport phenomena, based on the property of chirality, may not be supported by the edge modes. And indeed, using the explicit form of the wave function (145), we find that the contribution of each edge mode to the chiral (axial) current in the direction along the axis of the cylinder is identically zero at every point of the cylinder's interior:

$$j_z^5(x) = \bar{\Psi}_m^{\rm edge}(x)\gamma^5\gamma^z\Psi_m^{\rm edge}(x) \equiv 0. \quad (147)$$

Therefore, the total axial current due to the edge modes vanishes:

$$\langle J_z^5\rangle_{\rm edge} \equiv 0. \quad (148)$$

This property can be understood readily from properties of the MIT boundary condition (9) and the corresponding edge modes; in the negative infinite mass limit, the edge modes are located only at the surface of the cylinder, and thus the axial current vanishes everywhere except the surface. However, the value of the axial current at the surface also becomes zero due to the MIT boundary condition (9) as mentioned in Eq. (10).

[3]It is worth also mentioning that the contribution of the light edge modes to the chiral condensate is identically zero $\bar{\Psi}_m^{\rm edge}\Psi_m^{\rm edge} \equiv 0$ in the considered limit of large bulk fermion masses.

The density of the electric (vector) current generated by a single edge mode is, however, nonzero,

$$J_z = \int_{|x|\le R} d^2x_\perp j_z(x) = \int_{|x|\le R} d^2x_\perp \bar{\Psi}_m^{\rm edge}\gamma^z\Psi_m^{\rm edge} = \frac{k_z}{2\pi E_m^{\rm edge}}, \quad (149)$$

where the energy of the edge mode $E_m^{\rm edge}$ is defined in Eq. (142). The dimension of the current density (149) comes from the fact that we integrated the current over the cylinder cross section and used the normalization of the edge modes (29) with respect to the inner Dirac product (30). Since the electric current (149) is antisymmetric with respect to reflections, $k_z \to -k_z$, the net electric current in the state of thermal equilibrium is identically zero,

$$\langle J_z\rangle_{\rm edge} \equiv 0. \quad (150)$$

We remind the reader that we cannot generate a chiral imbalance with the edge modes since these modes are not chiral (146).

Thus, we come to the conclusion that anomalous transport phenomena, such as the chiral magnetic effect and chiral vortical effect, are not supported by the (massless) edge modes.

V. CONCLUSIONS

We study a uniformly rotating relativistic system of free Dirac fermions in the background of a constant magnetic field directed along the axis of rotation. The system must be bounded in any plane perpendicular to the rotation axis in order to respect the relativistic causality according to requirement that the rotational velocity of particles does not exceed the speed of light. Therefore, we enclose the system into an infinitely high cylinder of radius R and restrict the angular frequency Ω of rotation to the subluminal domain: $\Omega R < 1$. At the surface of the cylinder, we impose either the MIT boundary condition (9) or its chiral generalization (35), which is characterized by the chiral angle Θ. Both these conditions force the normal component of the fermionic current to vanish at cylinder's surface, thus conserving the global fermionic number inside the rotating cylinder.

In general, the spectrum of fermions in a finite geometry contains two types of solutions: bulk solutions concentrated in the interior of the system and the edge states which are localized at the boundary. The bulk states in cylindrical geometry were already discussed in the literature. In the absence of magnetic field, the bulk spectrum of fermions was obtained in Ref. [10], in which the cylinder with the MIT boundary conditions (9) was studied. The bulk spectrum with the chiral MIT boundary conditions (35) was found later in Ref. [18]. In our paper, we extend these results in various directions.

First, we find that the system possesses the edge modes at a certain region of the parameter space. Second, we extend the results for the edge and bulk modes to the case of nonzero magnetic field parallel to the axis of the cylinder (so that the magnetic flux is a constant quantity along the axis of the cylinder). Third, we implement the uniform rotation of the whole system and investigate the interplay between rotation and magnetic field in thermodynamical properties of free fermions.[4] Fourth, we highlight the role of the edge states that have been neglected so far in the analysis of thermodynamics of rotating fermionic systems.

We found the following features of the system:

(1) The boundary condition is important for the edge states. The mass spectrum and the very existence of the edge modes depend on the values of the fermion mass M, magnetic field B, and the chiral Θ angle at the boundary. For example, there are no edge states at the chiral angle $\Theta = \pi/2$ at zero magnetic field.

(2) The lowest (ground-state) bulk modes transform into the edge states and vice versa as the value of the fermion mass M crosses, for each fixed value of the angular momentum (17), a certain threshold mass. In the absence of magnetic field, the threshold masses (34) are given, for the MIT boundary conditions (9), by $M_c = -n/R$ with $n = 1, 2, \ldots$. They differ from the threshold masses for the fermions with the chiral boundary conditions (36). The threshold masses for the MIT boundary conditions are changed to Eq. (127) in the case of nonzero magnetic field.

(3) The edge states are massive so that in the solid-state language the system may be associated with a nontopological insulator.

(4) The masses of the edge states are finite for $B = 0$. In the absence of magnetic field, the spectrum is degenerate with respect to the sign flips of the angular momentum, $\mu_m \to -\mu_m$; see Fig. 2. The masses of the bulk (edge) modes rise (fall) with the increase of the absolute value of the fermion mass M. In the limit of a negative infinite fermionic mass, $M \to -\infty$, the bulk modes become infinitely heavy so that they decouple from the dynamics of the system and disappear. On the contrary, in this limit, the masses of the edge modes remain finite (76). They are proportional to the mean curvature of the cylinder's surface, $1/R$.

(5) The masses of the edge states may vanish for $B \neq 0$. Nonzero magnetic field lifts out the $\mu_m \to -\mu_m$ degeneracy of the mass spectrum of both the bulk states and the edge states; see Fig. 7. For example, the edge states with $\mathrm{sign}(\mu_m eB) > 0$ possess only nonvanishing masses, while the masses of the edge states with $\mathrm{sign}(\mu_m eB) > 0$ may become zero at certain values of momentum, shown in Fig. 8. The masses of the bulk modes become infinitely massive in the limit $M \to -\infty$, while the masses of the edge states exhibit a periodic dependence on the magnetic flux, see Fig. 9, described by the simple formula (133).

(6) The moment of inertia oscillates with magnetic field. The presence of magnetic field affects drastically the rotational properties of the system. For example, in the domain of low temperatures in the limit of infinitely large negative fermion mass—where the thermodynamics is given by the edge modes only—the angular momentum (Fig. 12) and, consequently, the moment of inertia (Fig. 13) experience quasi-periodic (quantum) oscillations as functions of magnetic flux ϕ_B. The local minima (maxima) of the moment of inertia correspond to the integer (half-integer) values of the magnetic flux ϕ_B in units of the elementary flux ϕ_0, Eq. (124). At high temperature, the oscillations disappear; see Fig. 13.

(7) Edge modes do not contribute to the anomalous transport of axial and electric charges. The edge modes do not possess a definite handedness in terms of chirality and helicity even in the case when these modes are massless. The edge states in the infinite negative mass limit cannot lead to anomalous transport phenomena such as the chiral vortical effect and/or chiral magnetic effect in uniformly rotating cylinder and/or in the background of magnetic field, respectively.

[4]Uniformly rotating fermions in magnetic field were also studied in Ref. [13] in a transversally unrestricted geometry which does not possess the edge modes.

ACKNOWLEDGMENTS

The authors are grateful to Pavel Buividovich, Mark Goerbig, and María Vozmediano for discussions. The work of S. G. was supported by the Special Postdoctoral Researchers Program of RIKEN. The research of M. N. C. was partly carried out within the state assignment of the Ministry of Science and Education of Russia (Grant No. 3.6261.2017/8.9).

[1] G. B. Cook, S. L. Shapiro, and S. A. Teukolsky, Rapidly rotating neutron stars in general relativity: Realistic equations of state, Astrophys. J. **424**, 823 (1994).

[2] L. P. Csernai, V. K. Magas, and D. J. Wang, Flow vorticity in peripheral high energy heavy ion collisions, Phys. Rev. C **87**, 034906 (2013); F. Becattini, G. Inghirami, V. Rolando, A. Beraudo, L. Del Zanna, A. De Pace, M. Nardi, G. Pagliara, and V. Chandra, A study of vorticity formation in high energy nuclear collisions, Eur. Phys. J. C **75**, 406 (2015); Y. Jiang, Z. W. Lin, and J. Liao, Rotating quark-gluon plasma in relativistic heavy ion collisions, Phys. Rev. C **94**, 044910 (2016); W. T. Deng and X. G. Huang, Vorticity in heavy-ion collisions, Phys. Rev. C **93**, 064907 (2016).

[3] D. T. Son and A. R. Zhitnitsky, Quantum anomalies in dense matter, Phys. Rev. D **70**, 074018 (2004); D. T. Son and P. Surowka, Hydrodynamics with Triangle Anomalies, Phys. Rev. Lett. **103**, 191601 (2009).

[4] A. Vilenkin, Quantum field theory at finite temperature in a rotating system, Phys. Rev. D **21**, 2260 (1980).

[5] A. Vilenkin, Parity violating currents in thermal radiation, Phys. Lett. **80B**, 150 (1978); Macroscopic parity violating effects: Neutrino fluxes from rotating black holes and in rotating thermal radiation, Phys. Rev. D **20**, 1807 (1979); M. Kaminski, C. F. Uhlemann, M. Bleicher, and J. Schaffner-Bielich, Anomalous hydrodynamics kicks neutron stars, Phys. Lett. B **760**, 170 (2016); N. Yamamoto, Chiral transport of neutrinos in supernovae: Neutrino-induced fluid helicity and helical plasma instability, Phys. Rev. D **93**, 065017 (2016).

[6] G. Basar, D. E. Kharzeev, and H. U. Yee, Triangle anomaly in Weyl semimetals, Phys. Rev. B **89**, 035142 (2014); K. Landsteiner, Anomalous transport of Weyl fermions in Weyl semimetals, Phys. Rev. B **89**, 075124 (2014); M. N. Chernodub, A. Cortijo, A. G. Grushin, K. Landsteiner, and M. A. H. Vozmediano, Condensed matter realization of the axial magnetic effect, Phys. Rev. B **89**, 081407 (2014).

[7] B. R. Iyer, Dirac field theory in rotating coordinates, Phys. Rev. D **26**, 1900 (1982).

[8] F. Becattini and F. Piccinini, The ideal relativistic spinning gas: Polarization and spectra, Ann. Phys. (Amsterdam) **323**, 2452 (2008).

[9] V. E. Ambruś and E. Winstanley, Rotating quantum states, Phys. Lett. B **734**, 296 (2014).

[10] V. E. Ambruś and E. Winstanley, Rotating fermions inside a cylindrical boundary, Phys. Rev. D **93**, 104014 (2016).

[11] A. Manning, Fermions in Rotating Reference Frames, arXiv:1512.00579.

[12] B. McInnes, Angular momentum in QGP holography, Nucl. Phys. **B887**, 246 (2014); Inverse magnetic/shear catalysis, Nucl. Phys. **B906**, 40 (2016); A rotation/magnetism analogy for the quark–gluon plasma, Nucl. Phys. **B911**, 173 (2016).

[13] H. L. Chen, K. Fukushima, X. G. Huang, and K. Mameda, Analogy between rotation and density for Dirac fermions in a magnetic field, Phys. Rev. D **93**, 104052 (2016).

[14] Y. Jiang and J. Liao, Pairing Phase Transitions of Matter under Rotation, Phys. Rev. Lett. **117**, 192302 (2016).

[15] M. N. Chernodub and S. Gongyo, Interacting fermions in rotation: chiral symmetry restoration, moment of inertia and thermodynamics, J. High Energy Phys. 01 (2017) 136.

[16] S. Ebihara, K. Fukushima, and K. Mameda, Boundary effects and gapped dispersion in rotating fermionic matter, Phys. Lett. B **764**, 94 (2017).

[17] G. Duffy and A. C. Ottewill, The rotating quantum thermal distribution, Phys. Rev. D **67**, 044002 (2003); P. C. W. Davies, T. Dray, and C. A. Manogue, The totating quantum vacuum, Phys. Rev. D **53**, 4382 (1996); O. Levin, Y. Peleg, and A. Peres, Unruh effect for circular motion in a cavity, J. Phys. A **26**, 3001 (1993).

[18] M. N. Chernodub and S. Gongyo, Effects of rotation and boundaries on chiral symmetry breaking of relativistic fermions, Phys. Rev. D **95**, 096006 (2017).

[19] S.-Q. Shen, W.-Y. Shan, and H.-Z. Lu, Topological insulator and the Dirac equation, SPIN **01**, 33 (2011).

[20] J. E. Moore, The birth of topological insulators, Nature (London) **464**, 194 (2010); M. Z. Hasan and C. L. Kane, Topological insulators, Rev. Mod. Phys. **82**, 3045 (2010).

[21] C. A. Lutken and F. Ravndal, Fermionic Vacuum fluctuations between chiral plates, J. Phys. G **10**, 123 (1984).

[22] L. D. Landau and E. M. Lifshitz, *Quantum Mechanics: Non-Relativistic Theory*, (Butterworth-Heinemann, Oxford, United Kingdom, 1981)

[23] N. M. Temme, *Asymptotic Methods for Integrals*, Series in Analysis (World Scientific, Hackensack, NJ 2015), Vol. 6.

[24] L. D. Landau and E. M. Lifshitz, *Statistical Physics, Part 1* (Butterworth-Heinemann, Oxford, 1980), Vol. 5.

[25] D. Jaksch and P. Zoller, Creation of effective magnetic fields in optical lattices: The Hofstadter butterfly for cold neutral atoms, New J. Phys. **5**, 56 (2003).

[26] G. Basar and G. V. Dunne, The chiral magnetic effect and axial anomalies, Lect. Notes Phys. **871**, 261 (2013); D. E. Kharzeev, Topology, magnetic field, and strongly interacting matter, Annu. Rev. Nucl. Part. Sci. **65**, 193 (2015).

[27] K. Fukushima, D. E. Kharzeev, and H. J. Warringa, The chiral magnetic effect, Phys. Rev. D **78**, 074033 (2008); A. Vilenkin, Equilibrium parity violating current in a magnetic field, Phys. Rev. D **22**, 3080 (1980).